2016-01-01

Combustion of Novel Thermite Mixtures for Iodine Generation

Sergio Emanuel Guerrero
University of Texas at El Paso, seguerrero7@gmail.com

COMBUSTION OF NOVEL THERMITE MIXTURES FOR IODINE GENERATION

SERGIO GUERRERO

Master's Program in Mechanical Engineering

APPROVED:

Evgeny Shafirovich, Ph.D., Chair

Arturo Bronson, Ph.D.

Cristian Botez, Ph.D.

Charles Ambler, Ph.D.
Dean of the Graduate School

Dedication

To God who's pulled me through the tough moments and gave me courage to go on, to my family who no matter what keep on believing that I can do more than what I deem I can, and to my friends and colleagues who push me to be at their level.

COMBUSTION OF NOVEL THERMITE MIXTURES FOR IODINE GENERATION

by

SERGIO EMANUEL GUERRERO

THESIS

Presented to the Faculty of the Graduate School of

The University of Texas at El Paso

in Partial Fulfillment

of the Requirements

for the Degree of

MASTER OF SCIENCE

Department of Mechanical Engineering

THE UNIVERSITY OF TEXAS AT EL PASO

May 2016

Acknowledgements

First and foremost, I would like to thank my research advisor and friend Dr. Evgeny Shafirovich for his constant guidance, support, and teachings throughout the term of this effort and further. Not only did he showed me how to become a better researcher and engineer but also a more professional individual. I appreciate every knowledge-full conversation.

I would also like to thank Dr. Bonnie Gunn for her support and advice on chemical analysis. I'm also very thankful to the peers that assisted me along the many subjects enclosed within the development of the experimental setup and the investigation done, in particular Miguel Solis, Virginia Jimenez, Emanuel Ochoa, Daniel Rodriguez, Armando Delgado and Alan Esparza.

Additionally, I would like to extend my gratitude to my friends and lab-partners Diego Delfin, Luis Chavez, Juan Duran, Alejandra Cabral, Sergio Cordova, Ricardo Martinez, Alberto Delgado, Gerardo Rodriguez and Luis Varela for their advice and support.

Last but not least, I thank my family for their support, encouragement, and faith in me to accomplish this and many more things. My parents who have provided me with the foundation pillars for everything I do, my brother who shows me admiration and who pushes me to be better, and my sister who fascinates me with her potential and gives me great hope for the generations to come.

This research was supported by the U.S. Department of Defense (Grants No. W911NF-12-1-0056 and No. W911NF-14-1-0034; Grant Officer's Representative: Dr. Ralph A. Anthenien of the Army Research Office; Co-GOR: Dr. Clifford D. Bedford of the Office of Naval Research).

Abstract

Halogen-containing reactive materials could be used for mitigating the spread of hazardous, active biological microorganisms aerosolized as a result of explosion. The present work exhibits experimental results on the combustion of mechanically alloyed aluminum-iodine (Al-I_2) powder mixed with Fe_2O_3, CuO, MoO_3, Bi_2O_3, and I_2O_5. Wet mixing was used to prepare the samples, which were then compacted into pellets and ignited with a CO_2 laser. A chamber was designed and built to accommodate for combustion and collection of products, and the available laser ignition setup was modified to enable combustion experiments with rapidly burning gas-generating mixtures. High-speed video recording was used for observation and analysis of the combustion process. Solid combustion products were collected for phase characterization by XRD as well as for chemical titration to determine the amount of released iodine. Mixtures of the Al-I_2 powder with Fe_2O_3 did not ignite, while mixtures of this powder with the other oxides exhibited a self-sustained propagation of the combustion front with similar burn rates. Comparison experiments with a finer, micron-sized Al powder have shown a more rapid combustion of mixtures based on metal oxides and, in contrast, a slower and unsteady combustion of Al/ I_2O_5 thermite. These observations were interpreted based on the analysis of reaction mechanisms. XRD analysis of solid combustion products for mixtures of the Al-I_2 powder with CuO, Bi_2O_3, and I_2O_5 revealed full oxidation of Al, which, however, may also be related to its oxidation by atmospheric oxygen. The chemical titration was used to analyze the combustion products of Al-I_2/I_2O_5 mixture and the results confirmed that the suitability of this method for quantifying iodine in combustion products of gas-generating mixtures.

Table of Contents

Acknowledgements v

Abstract vi

Table of Contents vii

List of Tables ix

List of Figures x

Chapter 1: Introduction 1

1.1 Introduction 1

1.2 Problem and purpose statement 1

1.3 Methodoly overview 3

Chapter 2: Literature Review 5

2.1 Introduction 5

2.2 Halogens as bacteria defeating agents 5

2.3 Thermites as delivery system for biocidal gases 7

2.4 Mechanically alloyed Al-I composite materials for iodine release 13

2.5 Summary 19

Chapter 3: Development of Experimental Setup.. 21

3.1 Introduction 21

3.2 Design objectives 22

3.3 Combustion chamber 22

3.4 Design safety calculations 26

3.4.1 Maximum allowed mass of sample for iodine-containing mixtures 28

3.4.2 Viewing window port 30

3.4.3 Laser window port 32

3.4.4 Chamber lids bolts 33

3.4.5 Conclusion 34

3.5 Electrical design 34

3.5.1 Photo-resistor laser sttopage 36

3.5.2 Relay and signaling light 43

3.5.3 Laser emergency power shutdown 44

3.6 Summary 45

Chapter 4: Experimental Procedure 47
4.1 Introduction....47
4.2 Sample preparation 47
4.3 Combustion experiments 49
4.4 Characterization of products....51
4.5 Chemical analysis 52
4.6 Summary....54
Chapter 5: Results and Discussion.. 55
5.1 Combustion behavior and characteristcs 55
5.2 Products characteriztion....57
5.2.1 Materials particle size....57
5.2.2 X-ray diffraction....59
5.2.3 Chemical analysis....61
5.3 Discussion....62
5.4 Summary....65
Chapter 6: Conclusion.. 67
References....69
Vita…….. 71

List of Tables

Table 2.3.1: Summary of measured parameters for various nano-thermites studied [20].....8

Table 2.3.2: Pressure cell data for studied thermite mixtures [17].....10

Table 2.3.3: Combustion test data for thermite samples [17].....12

Table 2.4.1: Iodine concentrations in the prepared materials from TGA (I_{TG}) and from quantitative X-ray analysis (I_{AlI3}) [10].....16

Table 3.4: Sample mass which increases the pressure in the chamber by 10 psig.....30

Table 3.5.1: Logic table for laser program part one.....40

Table 3.5.2: Logic table for laser program part two.....42

Table 5.1: Characteristics of studied thermite mixtures.....57

Table 5.2: Particle size distributions of used fuels and oxidizers.....59

Table 5.3: Adiabatic flame temperatures of the tested mixtures.....63

List of Figures

Figure 1.3: Schematic of combustion mechanism. 3

Figure 2.3.1: XRD patterns (Intensity vs. 2Θ) of pure AgIO3, unreacted Al/AgIO3, and reacted Al/AgIO3 [17]. 11

Figure 2.3.2: TEM image and 1D elemental linescan for Al+I_2O_5 combustion products [22] 13

Figure 2.4.1: TG decomposition traces of pure AlI3, I2, and sample studied [10]. 15

Figure 2.4.2: XRD patterns for mechanically alloyed Al-I material samples [10]....16

Figure 2.4.3: Inactivation of aerosolized BG spores by combustion of different materials [6]. ...18

Figure 2.4.4: Optically measured temperatures of some seeded hydro-carbon flames [6]. 19

Figure 3.1: Previous experimental setup. 21

Figure 3.3.1: Main body part of the combustion chamber. 23

Figure 3.3.2: Outside (left) and inside (right) views of the chamber lids. 24

Figure 3.3.3: Chamber tube extension for laser introduction and ZnSe glass protection. 25

Figure 3.3.4: Combustion chamber base (left) and thermite sample holder (right). 26

Figure 3.4: Combustion chamber on base (top). Combustion chamber ZnSe window port (bottom-left) and chamber interior (bottom-right). 27

Figure 3.4.1: Borosilicate window representation with experienced pressure. 31

Figure 3.4.2: Tube ZnSe window representation with experienced pressure. 32

Figure 3.4.3: Diagram representing the bolts on chamber and the forces on them. 33

Figure 3.5: Electrical connections diagram for experimental setup. 36

Figure 3.5.1: Photo-resistor placement on chamber (left) and battery for photo-resistor (right). .37

Figure 3.5.2: Diagram of electrical connection for the photo-resistor. 38

Figure 3.5.3: Laser LabView program user interface (top), and logic schematic for program (bottom). 39

Figure 3.5.4: Logic schematic for part one of the laser program. 40

Figure 3.5.5: Logic schematic for part two of the laser program. 41

Figure 3.5.6: Laser in-use revolving incandescent light. 43

Figure 3.5.7: SainSmart 5 V 2-channel solid state relay board. 44

Figure 3.5.8: Normally closed emergency kill switch. 45

Figure 4.2: Dry mixed powder in Bioengineering Inversina mixer (left), and wet mixed powder in Resodyn LabRam acoustic mixer (right). 49

Figure 4.3: Schematic of new experimental combustion setup. 50

Figure 4.4: Bruker D8 Discover XRD. 51

Figure 4.5.1: Schematic of vacuum filtration setup for combustion products solution. 52

Figure 4.5.2: Titration setup for combustion products solution. 53

Figure 5.1: Progressive combustion still images of iodinated *(*Al-I_2*)* thermite samples. (A) Fe_2O_3, (B) Bi_2O_3, (C) CuO, (D) I_2O_5, (E) MoO_3. 56

Figure 5.2.1: Particle size distributions of the used (a) fuels and (b) oxidizers. 58

Figure 5.2.2: XRD pattern of combustion products for Al-I_2/CuO samples. 59

Figure 5.2.3: XRD pattern of combustion products for Al-I_2/I_2O_5 samples. 60

Figure 5.2.4: XRD pattern of combustion products for Al-I_2/Bi_2O_3 samples. 60

Chapter 1: Introduction

1.1 Introduction

In the last decades, the increased threat of a chemical attack or a chemical/biological disaster has raised the interest of governments and individuals in the development of effective methods for neutralizing and mitigating such events. A chemical attack is the deliberate release of a toxic gas, liquid, or solid that can poison people and the environment [1]. Chemical weapons were first used in World War I even after being prohibited in the Hague Convention of 1907 [2]. The types of chemical weapons used ranged from disabling chemicals, such as tear gas and the severe mustard gas, to lethal agents like phosgene and chlorine. Since then, the spread of technical knowledge and achievements made in bio-technology has considerably increased the possibilities of bio-terrorism. Further, many of the complicated processes for obtaining chemical weapons have been simplified over the years, materials needed have also become more available and affordable, thus increasing the possibilities of an attack or disaster to happen.

The most fatal chemical attack recorded to date was in March 1988 in the Kurdish village of Halabja where a combination of mustard gas, Sarin and possibly Vx killed at least 5000 people and left more than 9000 others with severe skin and respiratory disorders [3]. The increased threat pose by such weapons has created an urgency to develop counter-measurements to mitigate and control the spread of such disasters and improve the bio-security globally.

1.2 Problem and Purpose Statement

Currently there are no counter-measures used to directly fight the bacteria or viruses released to the environment in chemical and/or biological disasters; instead, there are many regulations, rules, laws, and monitoring to prevent such events. Once an event has occurred, the procedure to follow consists mostly of assessing the damage, and assisting and treating those that have been exposed, i.e. quarantine, application of antidotes, and antibiotics. The government has tried using warheads [4] and explosives that generate high-temperature gases aiming to neutralize chemical and biological agents, but it has been shown that this method is not very effective as explosives and high thermal events alone cannot completely destroy biological agents [5, 6]; explosives lack the heat to burn off biological agents, and shock pressures

can disperse any remaining agents. It is desired to quickly destroy chemical/biological agents and prevent the further contamination and spread of the agents.

The need of an effective method for neutralizing and mitigating chemical and biological agents over a short period of time has led to the investigation and development of halogen-containing compositions, in particular iodine, containing energetic materials such as thermites. Thermites consist of a metal fuel and an oxidizer. When ignited, they exhibit a highly exothermic and self-propagating combustion reaction with a very high energy release. Aluminum is most often the choice of fuel owing to its high reaction enthalpy, high thermal conductivity, and availability. Halogens are well known for their biocidal properties, and their presence in the combustion products of an explosive charge is expected to significantly reduce the concentration of viable microorganisms, escaping from the high-temperature blast zone [7-8]. These compositions offer both a thermal and long-lasting biocidal agent release, which can be useful in inactivating biological materials [5, 9]. A problem faced with these compositions is that they are mostly nano-compositions which are known to be extremely reactive, so that their handling and storage become a challenge.

More recently it was demonstrated that the use of mechanical milling facilitated the preparation of a stable at room temperature aluminum-iodine composite [10]. Relatively low ignition temperatures of this powder [11-12] imply that it can substitute aluminum in thermite mixtures, thus serving as a fuel and, at the same time, the source of iodine. At the same time, this material is a micron-sized powder and it is easy to store and handle it as compared with nanoscale aluminum. It is expected that the use of this material instead of aluminum in thermite mixtures based on iodine-containing oxides will increase iodine yield, while maintaining the mixture's high energy density. Further, thermite mixtures of Al-I_2 powder with oxides of metals such as iron, copper, bismuth, and molybdenum could be used for iodine generation when relatively small amounts of iodine are sufficient and the use of unstable and hygroscopic iodine-containing oxides is not desired.

The objective of this thesis is to investigate the combustion of thermite mixtures composed of the mechanically alloyed Al-I_2 powder with the following oxides: Fe_2O_3, CuO, MoO_3, Bi_2O_3, and I_2O_5. For base control and comparison purposes, combustion characteristics of these mixtures are compared with

those of thermites based on commercial, micron-sized Al powder. It is also of interest to characterize the combustion products of iodine-containing thermites and explore methods for quantifying the amount of iodine released during combustion.

1.3 Methodology Overview

The selection of oxidizers for this study was based on a list of the most studied oxidizers in thermite reactions [13-14]. The mixtures of Al-I_2 and oxides were prepared based on stoichiometric ratios of the reactions between Al and oxides, while iodine was considered as an inert component.

The first step in the development of the experimental procedure was to find an effective standard method of mixing for the thermite compositions, one that could provide an agglomeration free powder product. Second step was the design and construction of an experimental setup which would allow both, the study of the combustion behavior and characteristics, and the collection of combustion products for characterization and quantification analysis of iodine-containing products.

The combustion experiments were conducted with pellets composed of the various fuels and oxides compositions. The pellets were ignited inside a combustion chamber with a CO_2 laser beam introduced into the chamber through a ZnSe window. In this process, the laser heats up the top of the pellet until ignition is reached; then, as the pellet is burning, the contained iodine is sublimated and released as gas into the surroundings (Fig. 1.3).

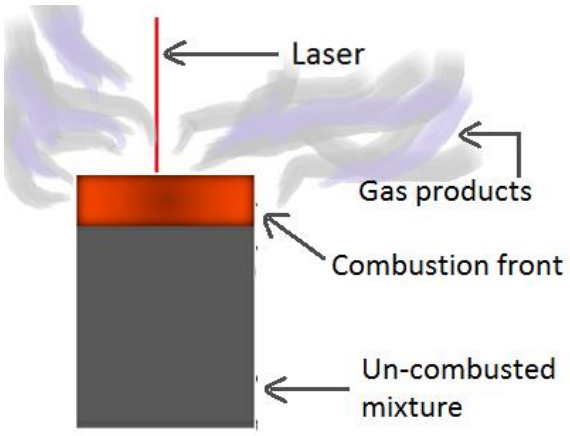

Figure 1.3: Schematic of combustion mechanism

Investigation of the combustion front velocity and visualization of the combustion wave propagation were obtained using a high speed video camera. The quantification analysis of iodine was performed by collecting the condensed combustion products and using chemical titration with sodium thiosulfate as the titrant.

Chapter 2: Literature Review

2.1 Introduction

New alternatives for neutralization and containment of biological micro-organisms have been of interest in recent years. The investigation on the inactivation of airborne micro-organisms with the use of not only thermal but chemical processes has gained significant attention. As described in the previous section, the use of weapons that provide short live thermal events might not be the most effective option when the purpose is to control or mitigate the spread of biological micro-organisms in the environment; it has been shown that the use of highly energetic reactive materials alone is not enough to completely defeat spore-forming bacteria [15]. Some bacteria might survive the explosion and heat of the fire from conventional weapons. The surviving bacteria agents could easily be transported in the atmosphere and contaminate larger surrounding areas posing a threat to the public in them. Thus it is of great importance to develop a method for neutralizing and mitigating biological agents within a short period of time after initiation, ideally a method which could work to defeat the bacteria during and after combustion.

Recently the idea of incorporating halogens into energetic materials has been considered a valuable approach to the effective inactivation of aerosolized micro-organism making use of the biocidal properties found in halogens. Nano- and micro-composite materials with halogen combinations have been explored because of their potential to defeat pathogenic airborne bacteria and in some instances viruses [11]. The use of highly energetic mixtures, such as thermites, combined with halogens and other biocidal agents, have been found a viable approach to the mitigation of aerosolized agents [5]. More recently, the capabilities of mechanical alloying have been explored leading to a new approach where halogens are combined with aluminum, a metal fuel commonly used for reactive mixtures, with the aim of having a greater impact on the defeat of airborne bacteria and viruses.

2.2 Halogens as bacteria defeating agents

Studies have demonstrated the capabilities of halogens such as iodine to effectively inactivate thermal-stress resistant airborne micro-organisms. As stated in the section above, the use of halogens as biocidal agents in combination with high temperatures of combustion has been of interest and recently

investigated as a new approach for mitigating and defeating airborne bacteria, even though it is important to better test and demonstrate the efficiency of such halogens at inactivating biological micro-organisms.

Grinshpun et al. [7] have developed an experimental technique for investigating the inactivation of airborne viable micro-organisms exposed to combustion of various materials over a short period of time, 0.01-1s. The goal was to demonstrate the results of using iodine in combustion as a biocidal agent to inactivate bacteria spores in contrast to inactivation results of bacteria's simple exposure to high temperatures of combustion environments. It was reported that this method is capable of quantifying viability loss (VL) of about 99.998%.

More specifically, in [7] nano-composite powders composed of Al fuel and MoO_3 oxidizer were prepared by arrested reactive milling and mixed with iodine. This mixture was fed into a gaseous oxygen-hydrocarbon flame (CH_4/N_2). The resultant flame was introduced into the test chamber where subsequently Bacillus atrophaeus spores were aerosolized at a constant flow rate. After exposure, the bio-aerosol particles were collected for analysis, which compared the organism's concentrations with and without exposure to the treatment.

Viability loss represents the deficit of ability of a living organism or system to maintain itself alive or recover its potentialities. To determine viability loss, first an inactivation factor (*IF*) was determined as:

$$IF = \frac{C_{culturable}(Control)}{C_{culturable}(Test)} \tag{2.1}$$

where the $C_{culturable}$ (*Control*) represents the concentration of micro-organisms measured without exposure and $C_{culturable}$ (*Test*) is the concentration measured with exposure. The viability loss (*VL*) is then obtained with Equation 2.2, presented below. If *IF* value is high, it means the inactivation of the bacteria is high and the viability loss is also high.

$$VL = \left(1 - \frac{1}{IF}\right) \times 100\% \tag{2.2}$$

Reported results revealed that the bacteria spore exposed to the burning $12Al{\cdot}MoO_3$ nanocomposite with no iodine produced relatively low IF-values: geometric mean (GM)= 52.3, whereas the solid-strand combustion of the same nanocomposite with embedded iodine produced much higher IF-values: GM = 9,849 [7]. The values obtained for iodine containing nano-composite revealed much higher inactivation levels, thus pointing to the effect that iodine had on the airborne bacteria spores as they passed through the test chamber. This results show the feasibility of iodine containing materials for application in the defeat of biological agents.

Bless et al. [15] also demonstrated the inactivating capabilities of iodine containing materials over microbial agents. Test tubes with aqueous solutions containing Bacillus atrhophaeus were evaporated leaving the bacteria at the bottom of the tubes. Next, a tube with the bacteria was placed inside a biocidal reaction chamber (BRC) along with thermite powder. Three oxidizers with known biocidal properties and one without them were studied in this effort. Specifically, iodine pentoxide (I_2O_5), silver oxide (AgO), and silver iodate ($AgIO_3$) were the biocidal oxides and iron oxide (Fe_2O_3) was the control non-biocidal one. The metal fuel for all oxidizers was nano-aluminum. The thermite powder was ignited with a nickel-chromium wire. The exposure time of the bacteria to the biocidal containing material combustion was much longer than in [7]: the bacteria was left in the chamber for one-hour exposure. After removing from the chamber, the bacteria were analyzed for growth after 24 and 48 hours, and growth rate was compared to the control sample that was not exposed to the reaction. It was reported that the iodine pentoxide is extremely effective at neutralizing the bacteria after only an hour of exposure time, whereas silver and iron oxide showed no sign of bacteria neutralization after this exposure time [15]. These results again demonstrate the efficacy of iodine and iodine-containing materials in the neutralization and inactivation of airborne or grounded bacteria.

2.3 Thermites as delivery system for biocidal gases

In the previous section, it was shown how thermite mixtures could be of use for the transportation and delivery of biocidal components such as iodine into a designated location or point of interest for the defeat of harmful biological microorganisms. Thermites are pyrotechnic compositions of a metal fuel and a metal oxide which, when ignited, undergo an exothermic reduction-oxidation reaction; these reactions

provide extremely high temperature events. One of the oldest and well known applications for thermites is thermite-welding, used in particular for joining railroad tracks. Since the discovery of thermite reactions back in the 1890s [16], mixtures of metal fuels and oxide powders have been used for their capabilities to release heat and pressure waves through their exothermic reactions. More recently, major attention has been gained, and progress has been made in the use of these highly-exothermic reactive mixtures as chemical air treatment methods, e.g. as gas generators, in particular by the addition of biocidal additives to combat the growth and spread of airborne bio-threat agents [5, 17].

Mostly aluminum is used as the primary metal fuel in thermites because of its nearly ideal properties for these reactions. Aluminum has a relatively low melting point (660°C), a high boiling point (2519°C) which enables the reaction to reach very high temperatures, and it is one of the cheapest highly reactive metals; aluminum also forms a passivation layer making it safer to handle than many other reactive materials [18].

A great advantage of using thermites is the ability to adjust the characteristics of the reaction such as energy density, power release, and pressure generation by the proper choice of combinations of fuels, oxidizers, material geometries, and reactant compaction [19]. Investigation has been done on various combinations of Al/oxide systems in the aim of identifying the most effective pressure and gas release systems. In 2014, Glavier et al. [20] investigated the burning rates and the pressure generation capabilities of 4 kinds of thermite powder mixtures prepared using nano-scale aluminum mixed with 3 different oxidizers (Bi_2O_3, CuO, MoO_3) and PTFE (Polytetrafluoroethylene). It was found that all mixtures produced pressure through gas release. The highest pressure peak was generated by CuO (41.7 MPa), while the maximum pressurization rate was seen for Bi_2O_3 (~5762 kPa/μs), also it was discovered that both Bi_2O_3 and CuO had the shortest delay time to reach the maximal pressure, 5 μs and 15 μs, respectively. Results found are shown in Table 2.3.1.

Table 2.3.1: Summary of measured parameters for various nano-thermites studied [20].

Thermite (30% TMD)	Delay time (μs)	Burning rate ($m \cdot s^{-1}$)	$P \times V/m_{Al}$ ($kPa \cdot m^3 \cdot kg^{-1}$)	Pressurization rate ($kPa \cdot \mu s^{-1}$)	P_{max} (MPa)
Al/Bi_2O_3	5	420	88	5762	21.6
Al/CuO	15	340	60	172	16.7
Al/MoO_3	110	100	25	35	7.4
Al/PTFE	550	2	33	27	21.4
Al/CuO foils	100	65	32	54	10

Glavier et al. found that the maximum pressure is strongly associated with the capability of the thermite to release oxygen and with the vaporization temperature of the metal fuel rather than the exothermicity of the reaction, as the pressurization is due to the release of several gas species which depend on the degree of completion of the reaction [20]. From their results, it can be concluded that gas generators based on bismuth and copper oxides possess desirable performances for thermite gas generating systems.

The rising attention to thermite mixtures incorporated with biocidal elements has led researchers to investigate the characteristics of these compositions with varied biocidal additives combinations [21, 17]. It is of importance to understand the way biocidal agents such as iodine and silver interact with energetic systems, i.e. determine how the reaction and combustion mechanisms of such mixtures are affected by biocidal additions and how effective these systems are in releasing the proper chemical form of biocidal element necessary to inactivate bacteria spores.

Silver iodate has recently been considered as a potential oxide for use in thermite-based biocidal applications because of its biocidal properties (Johnson et al., 2008). Sullivan et al. [17] conducted an investigation on the combustion performance and the final state of the products for $Al/AgIO_3$ nano-thermites. Rapid heating wire experiments and constant volume combustion tests were performed in order to measure the burning rate and ignition temperatures; also the reacted products of this mixture were examined using X-ray diffraction and electron microscopy to determine composition and morphology. After hot wire combustion experiments, it was found that the ignition temperature of stoichiometric $Al/AgIO_3$ in air at atmospheric pressure was 1215 ± 40 K. For comparison, the ignition temperatures of Al/Fe_2O_3 and Al/CuO were also measured under the same conditions and these were found to be 1510 ± 40 K and 1220 ± 40 K, respectively. For the pressurization results, it was found that $Al/AgIO_3$ significantly outperforms both Al/Fe_2O_3 and Al/CuO, achieving a much higher peak pressure and pressurization rate. The results are shown in Table 2.3.2. These results were attribute to the decomposition products of the oxidizer as $AgIO_3$ can release significantly more gas upon thermal decomposition, i.e. O_2, O, and I.

Table 2.3.2: Pressure cell data for studied thermite mixtures [17].

	Al/Fe_2O_3	Al/CuO	$Al/AgIO_3$
Pressure rise (psi)	13.4	116	296
Pressure rise time (μs)	800	13	5.3
Pressurization rate (psi/μs)	0.017	9.0	57
FWHM burn time (μs)	936	192	172

Lastly, XRD diffraction analysis and transmission electron microscopy (TEM) were used for characterization of the combustion products. XRD patterns for un-reacted and reacted $Al/AgIO_3$ powders were obtained for comparative analysis. The XRD results are shown in Figure 2.3.1. It was observed that for the reacted powder, Al and $AgIO_3$ spectra disappeared and AgI emerged as the foremost peak in the pattern. Neither elemental silver nor iodine was detected by XRD and apparently AgI was the only biocidal reaction product of $Al/AgIO_3$. The TEM analysis identified micro-sized aluminum oxide, ≤ 100 nanometer AgI particle, and some micro-sized islands of elemental Ag; this results supported the XRD findings of AgI as the predominant product.

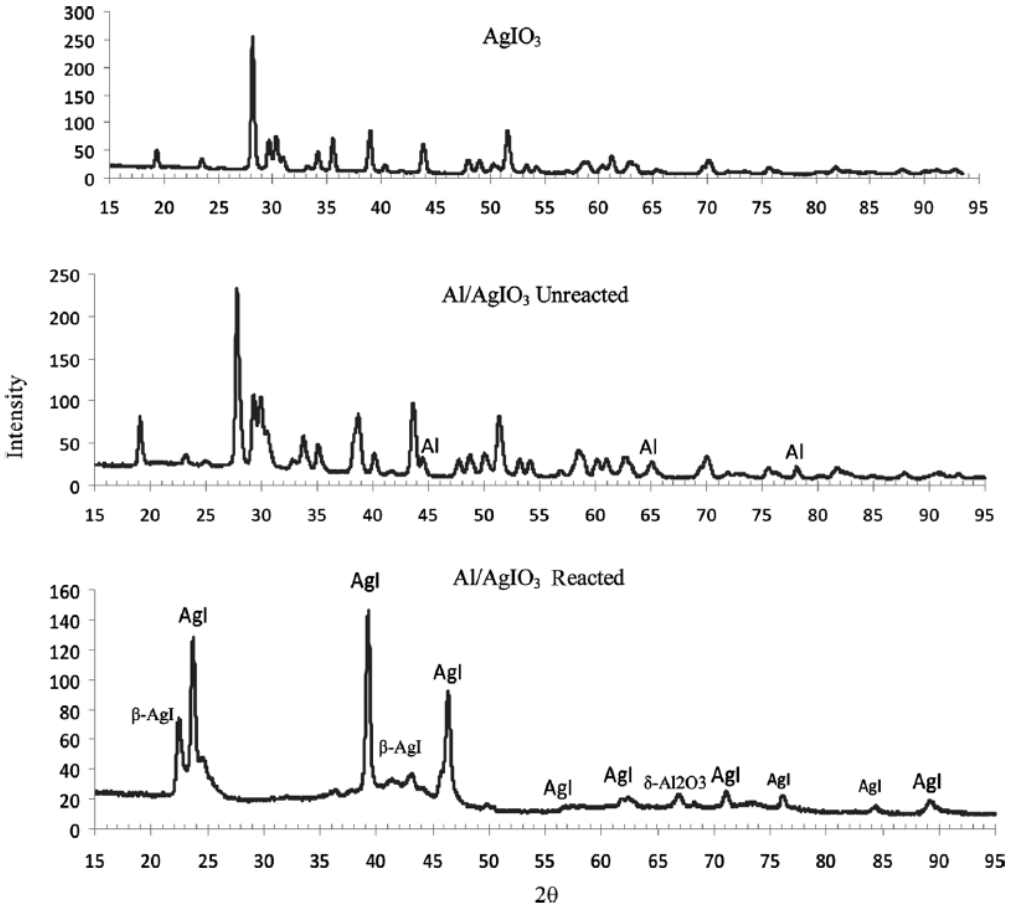

Figure 2.3.1: XRD patterns (Intensity vs. 2Θ) of pure $AgIO_3$, unreacted Al/$AgIO_3$, and reacted Al/$AgIO_3$ [17].

On another effort, Jian et al. [22] investigated the ignition and combustion of nano-Al/micro-I_2O_5 thermite, and also studied its potential use in biocidal applications by analyzing the reaction's products. As in the previous investigation by Sullivan et al., rapid heating wire ignition and constant volume combustion tests were carried out to characterize the pressure rise during combustion. The post-combustion products were analyzed by TEM equipped with energy dispersive X-ray spectrometer (EDS) for elemental analysis.

The combustion experiments were conducted in atmospheric conditions. The ignition temperature of Al/I_2O_5 system was found to be ~810 K. For performance comparison, the combustion processes of Al/CuO and Al/Fe_2O_3 thermites were also studied under the same conditions. The results of these

experiments are summarized in Table 2.3.3. It is seen that I_2O_5 exhibits the highest over-pressure and pressurization rate as well as shortest burning time when compared to the other Al/micro-oxide systems.

Table 2.3.3: Combustion test data for thermite samples. All oxidizers mixed with nano-Al [22].

Oxidizers (w/Al, φ=1)	**P_{rise} (KPa)**	**Pressure rise time (μs)**	**Pressurization Rate (KPa/μs)**	**FWHM burn time (μs)**	**Note**
I_2O_5 (A)	237	944	0.251	1579	As received, Sigma-Aldrich, 99.99 %
I_2O_5 (M)	366	397	0.922	293	After 1 hour milling
Micro-CuO	152	732	0.208	514	<5 μm, 98% ,Sigma-Aldrich
Micro-Fe_2O_3	51.7	8350	0.00619	4394	<5 μm, ≥99%, Sigma-Aldrich
Nano-CuO	800	13	61.5	192	<50 nm, Sigma-Aldrich
Nano-Fe_2O_3	92.4	800	0.116	936	<50 nm, Sigma-Aldrich

A thermodynamic equilibrium analysis was conducted for Al/Fe_2O_3, Al/CuO, and Al/I_2O_5 thermites [23], in which it was shown that thermites based on Cu and I have a higher capacity to release gas relative to Fe based thermites (Cu - 5.4 mmol/g, I – 6.3 mmol/g, and Fe – 1.4 mmol/g). These results are consistent with the pressurization data presented in Table 2.3.3, where the pressure rise and rate are higher for I_2O_5 and CuO than for Fe_2O_3 based systems.

A TEM analysis of the combustion products using energy-dispersive X-ray spectroscopy (EDS) provided an elemental map that indicated the presence of particles containing Al, O, and I. A TEM image and 1D elemental linescan are shown in Figure 2.3.2. It was concluded that Al/I_2O_5 thermite reactions are an effective way to produce iodine gas. Furthermore, upon cooling, the iodine condenses to form high surface area nano-particles, thus maximizing its biocidal potential.

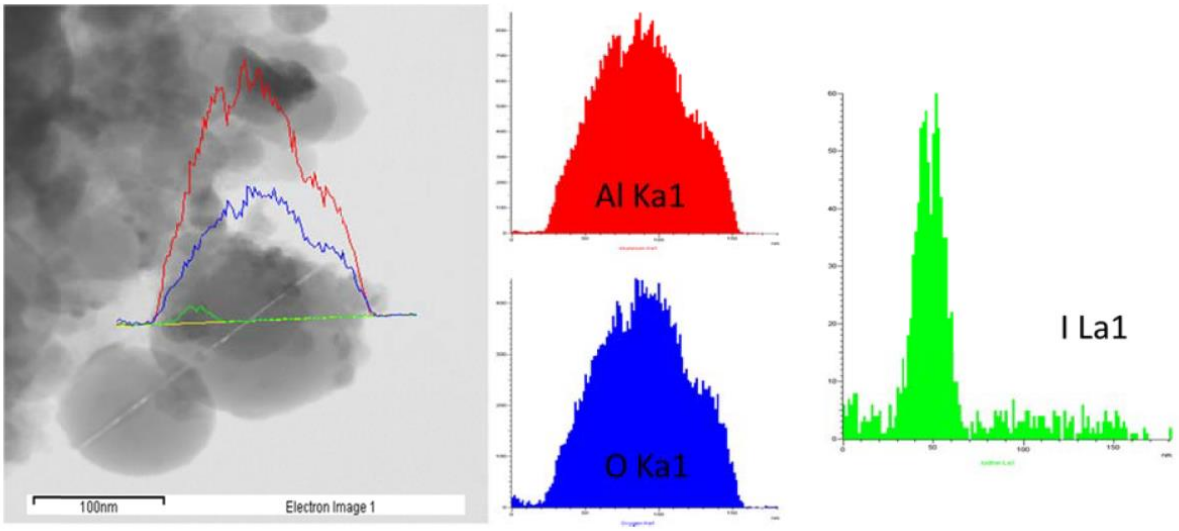

Figure 2.3.2: TEM image and 1D elemental linescan (using EDS) for Al+I_2O_5 combustion products [22].

2.4 Mechanically alloyed Al-I composite materials for iodine release

In the previous section, the approach of using energetic materials such as thermite mixtures was reviewed and it was shown that various research efforts demonstrated the performance and feasibility of their use for iodine release and, in turn, for bacteria inactivation. In all of the cases presented before, the biocidal additive was embedded into or was part of the metal oxide in the thermite; this resulted as an effective way of releasing the additive, especially for thermites based on I_2O_5 as the oxidizer [22]. Also, it is important to note that most of the reactive compositions studied for these applications consisted of nano-sized powder components. This brings a series of difficulties as these materials are extremely reactive and their compositions are typically very easy to ignite, so that their handling and storage becomes a challenge.

In recent years, a new approach to the transport and release of biocidal agents has been of interest for investigation. This approach involves metal-based composites containing halogens stabilized at room temperature; these composites could be used as the metal fuel additive to a thermite mixture. In particular, it is of interest to incorporate halogens into aluminum because of widespread use of the latter in energetic

formulations. In this method, the halogen-modified Al powder has characteristics similar to those of regular Al powder, such as high material and energy density, therefore burning in a similar form, but it also produces biocidal products during combustion. Furthermore, the development of this composite broadens the list of possible oxidizers combinations that can be used for thermite formulations; this is important given that every Al/oxide combination performs in a different manner as explored earlier in section 2.2 of this chapter.

The development of an Al/I composite material was achieved in 2010 by Prof. Dreizin's team at the New Jersey Institute of Technology [11]. Mechanically alloyed aluminum-iodine composites with iodine concentrations of more than 10 wt % were prepared from elemental aluminum and iodine. Powders of Al-I composites were prepared by ball-milling. Various milling environments and cooling agent combinations were tested, but the method found to be the most effective at preparing stabilized Al-I compounds was having liquid nitrogen flushed through the cooling jacket of the milling vial, and gaseous nitrogen fed into the milling vial [10]. Samples were found to consist of micrometer-sized particle, a particle size distribution analysis revealed a mean volume diameter (d_{mv}) of 21.3μm. The release of iodine upon heating was studied by a thermogravimetric analysis (TGA) which characterized the mass reduction of a mechanically alloyed sample, pure iodine, and AlI_3 for reference and comparison. The results shown in Figure 2.4.1 demonstrate that pure iodine evaporates completely before reaching 200°C, AlI_3 starts decomposing at room temperature, then the decomposition rate increases at around 200°C when AlI_3 melts, and most of it decomposes before temperature reached 400°C. In contrast, the mechanically alloyed sample shows a very small mass loss until the temperature reaches about 440°C, while the highest rate of mass loss occurs around Al melting point.

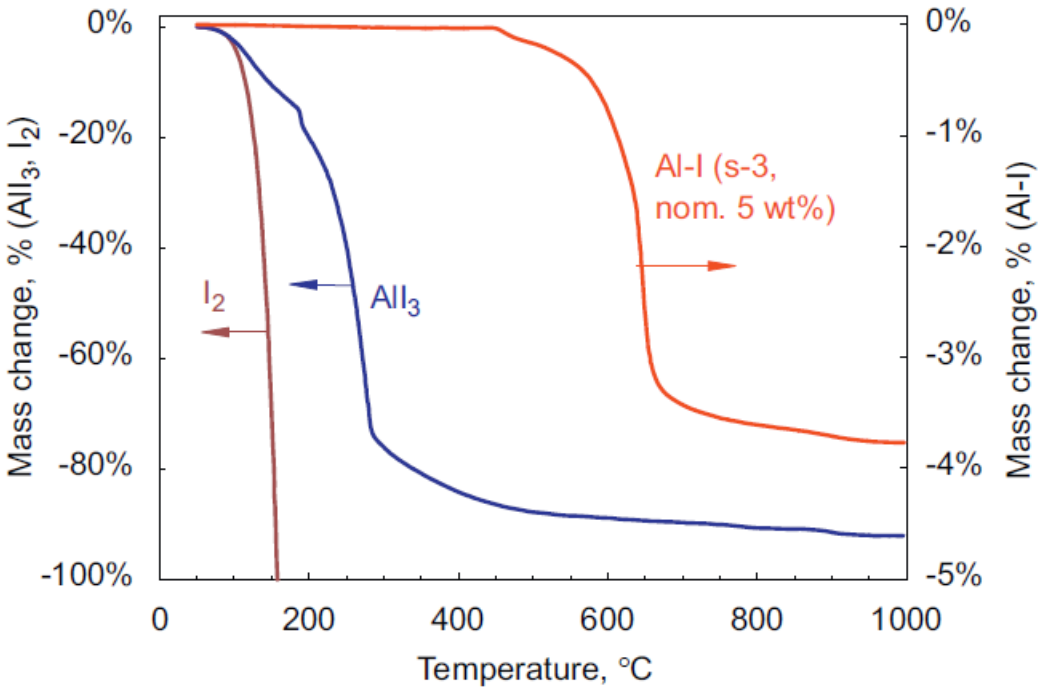

Figure 2.4.1: TG decomposition traces of pure AlI_3, I_2, and sample studied [10].

Through various TG analysis of the mechanically alloyed samples it was also discovered that upon ignition, iodine release occurs in two main stages. The first mass loss stage starts around 100°C and ends approximately at 350°C, this stage correlates with the respective temperatures at which pure iodine and AlI_3 were observed to evaporate upon heating, see Figure 2.4.1. The second stage of mass loss was observed to begin at around 400°C and continues until the sample reaches the Al melting point, at this point it is apparent that nearly all iodine captured in the material has been released.

An XRD analysis (see Fig. 2.4.2) has shown that Al and AlI_3 had the most consistent representation in all the samples studied. The peaks of AlI_3 are broad for most samples indicating that AlI_3 is not well crystallized. The XRD results were analyzed by whole-pattern refinement using the GSAS software package [24], the measured patterns were fitted with calculated patterns assuming the composition to include only two components, Al and AlI_3. Using TG results, it was found that for most samples more than half of the iodine is not contained in the AlI_3 detectable by XRD. These results are presented in Table 2.4.1.

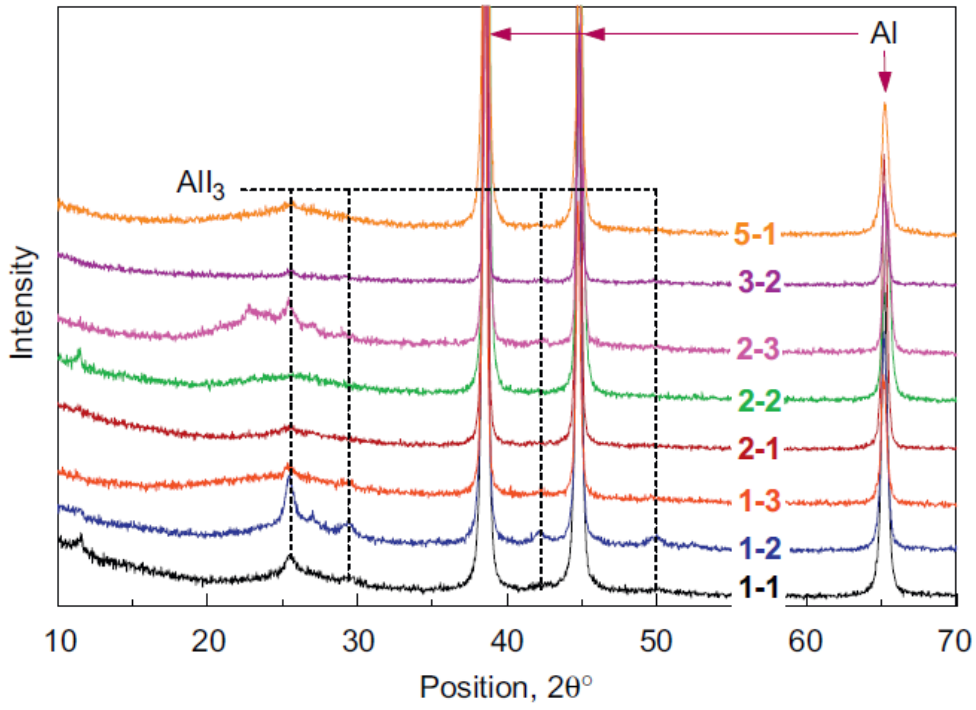

Figure 2.4.2: XRD patterns for mechanically alloyed Al-I material samples [10]

Table 2.4.1: Iodine concentrations in the prepared materials from TGA (I_{TG}) and from quantitative X-ray analysis (I_{AlI3}) [10].

Sample ID	Wt. fraction of I loaded, I_0, %	Total TG mass loss, I_{TG}, %	XRD whole-pattern processing: wt. fraction of I in AlI_3, I_{AlI_3}, %	Iodine balance (unaccounted for), $(I_{TG} - I_{AlI_3})/I_{TG}$, · 100%
1-1	5	4.56	1.59	65.1
1-2	10	8.01	4.02	49.8
1-3	20	15.53	3.18	79.5
2-1	5	4.62	1.60	65.4
2-2	10	7.53	3.24	57.0
2-3	20	16.49	4.52	72.6
5-1	10	8.37	3.75	55.2

In summary, mechanically alloying was found to be an effective method for preparation of Al-I composites in which iodine is bonded to aluminum and is not released until the material is brought to high temperatures. Milling at liquid nitrogen temperatures was found to be effective in preparing stabilized Al-I compounds. It was found that, upon heating, iodine was released in two stages meaning that it formed two bonds: a weak bond which volatizes similarly to elemental I and AlI_3, and a strong bond in which iodine is retained in aluminum until the material is heated up to nearly the Al melting point. And although

AlI_3 was found to be persistently present in the products, TG measurements helped reveal that AlI_3 decomposed almost completely upon heating to 400°C and that less than 10% of the entire iodine retained in stabilized mechanically alloyed powders was released upon heating to this same temperature, meaning that other iodine compounds remained in the samples bonded to Al stronger than in AlI_3, so that their thermal decomposition and release occur at higher temperatures.

Thus the preparation and capabilities to release iodine from this new alloyed composite, Al-I, have been explored, but it is also important to determine how effective this material is at inactivating and mitigating biological agents. This aspect was investigated by Grinshpun et al. [6], where the efficiency of halogen-containing reactive materials to inactivate aerosolized bacteria and viruses was determined. Spores of Bacillus atrophaeus and MS2 viruses dispersed in dry air were exposed for sub-second time intervals to hydro carbon flames seeded with various reactive powders so that bio-aerosol particles interact with the combustion products in a controlled high-temperature environment. The experiments were designed to quantify differences in the biocidal effects of the various reactive materials studied. These powders included: micro-Al (3-4.5μm), Mg (44μm), B-Ti nanocomposite, 8Al-MoO_3 nano-thermite, and novel Al-I_2 nano-composite.

The experimental setup for testing was very similar to the one used in Grinshpun et al. [7]. A vertical cylinder channel served as the exposure/combustion chamber, a seeded hydrocarbon flame placed in the center along the axis of the chamber was generated using a burner, a pushed rod introduced the powder into the flame for testing, and the bacteria were aerosolized from the bottom of the chamber alongside the burner; more details on the setup can be found elsewhere [6, 7]. The bacteria inactivation analysis was similar to the one performed by Grinshpun et al. [7] and described earlier in Section 2.2. It was done by comparing the organism's concentration with and without exposure to the treatment, with the inactivation factor (IF) being used to determine viability loss.

Results found for inactivation are presented in Figure 2.4.3. Inactivation factors for airborne BG spores exposed only to the powder-free hydrocarbon flame were determined to be [GM (GSD)]: 50 (1.49), where GM is the geometrical mean and GSD is the geometric standard deviation. Combustion of non-iodinated materials was found to produce inactivation factors [GM (GSD)] ranging from 231 (108) for

8Al-MoO_3 to 857 (361) for Al. This showed that powder combustion even without iodine increases the spore inactivation greatly as compared to pure hydrocarbon flame. The aluminum-iodine composite achieved a much more effective inactivation of airborne spores compared to non-iodinated powder; the inactivation factor was found to exceed 15,000.

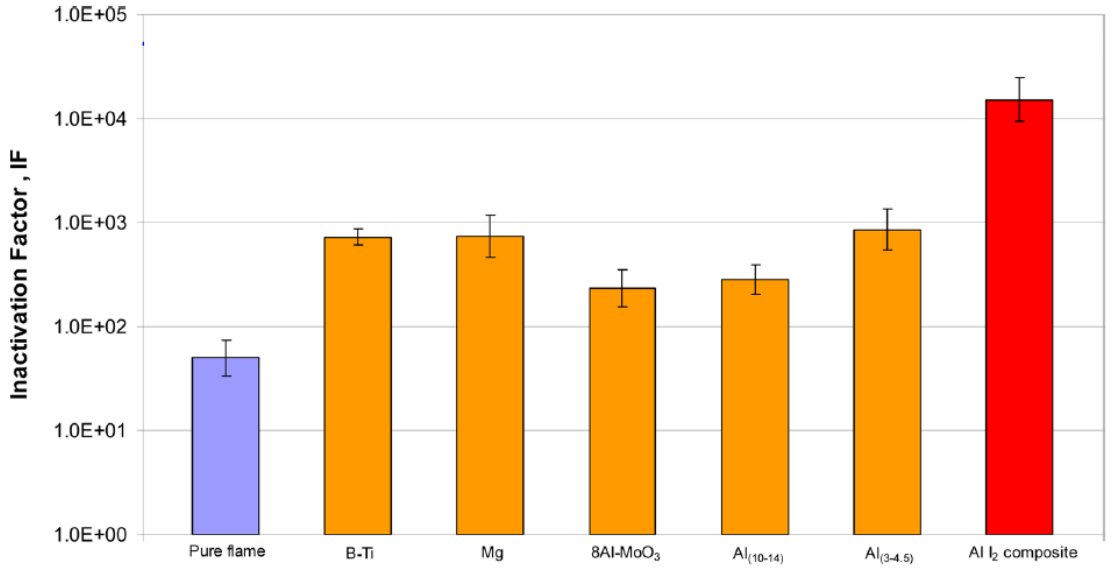

Figure 2.4.3: Inactivation of aerosolized BG spores by combustion of different materials [6].

The flame temperature of some of the tested reactive powders was optically measured using a calibrated UV/Visible spectrometer (StellarNet EPP2000). The results (see Fig. 2.4.4) have shown that the temperature of the Al-I_2 nano-composite is only a little higher than the one of pure Al which was of comparable size. This indicates that the enhanced inactivation demonstrated by the iodine bearing nano-composite is caused not by temperature effect but rather by the release of iodine.

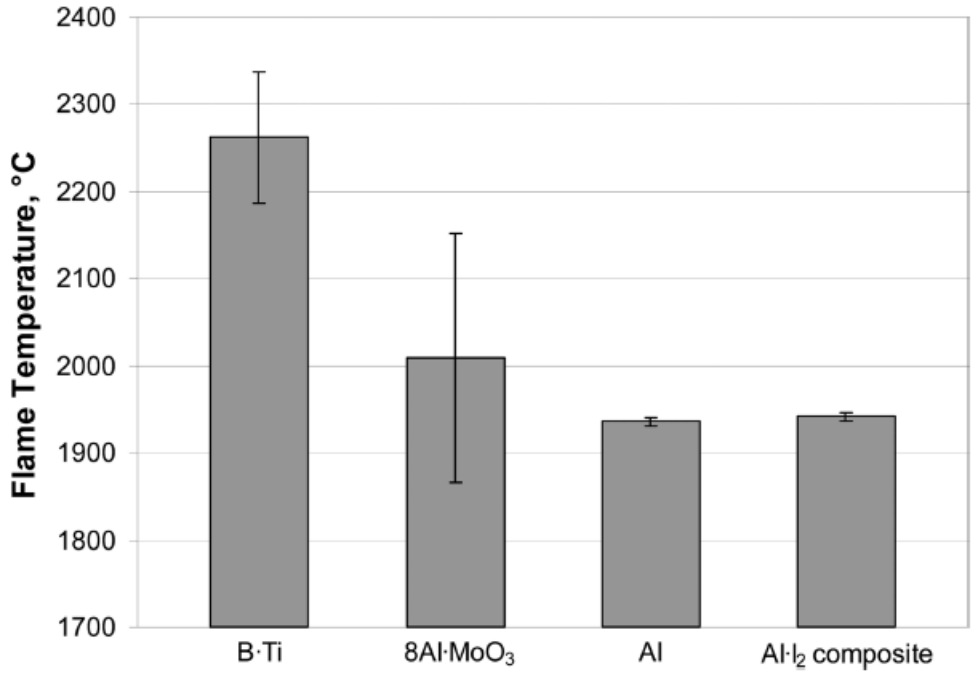

Figure 2.4.4: Optically measured temperatures of some seeded hydro-carbon flames [6].

In addition, the aerosolized virus MS2 was effectively inactivated by the exposure to both: the combustion products of the powders and to the pure hydrocarbon flame. From the overall results, this effort exhibited the great potential of combustion products generated by iodine-containing Al nano-composite materials for the inactivation of aerosolized micro-organisms.

2.5 Summary

Research efforts to find a more effective method for neutralizing biological threats have led to the use of halogen-containing compositions because of their known biocidal properties. Studies demonstrated the capabilities of iodine for inactivating stress-resistant airborne bacteria. When imbedded in an Al/MoO_3 mixture and introduced into a high-temperature environment containing Bacillus atrophaeus spores, the products showed an inactivation factor (IF) of more than two orders of magnitude greater than the effects of Al/MoO_3 without iodine.

Thermite compositions were found to be effective transport and delivery systems for biocidal elements, specifically, iodine and silver. Their capabilities to generate high thermal events and pressure waves, as well as ability to regulate the reaction by selecting the appropriate combination of fuel and oxidizer make them a suitable tool in chemical air treatment such as biocidal gas generators. It was found that the addition of biocidal elements to thermite mixtures did not greatly affect the combustion mechanisms and characteristics, e.g., ignition temperature and pressurization properties. In some cases, the pressurization performance was better, which was accredited to the release of halogen gases. Also, elemental maps of the combustion products of iodine-containing thermites demonstrated the presence of pure iodine particles with high surface area.

The novel mechanically alloyed Al-I composite was shown to be efficient in containing and retaining iodine at room temperatures and then releasing it when the composite is put to higher temperatures. Its micrometer particle size also makes it a much safer material to handle and store compared to nano-scale aluminum. This composite was also found to be effective for inactivating bacteria upon ignition; compared to flame mitigation and reactive material powders, Al-I_2 composite demonstrated an inactivation factor of at least two orders of magnitude greater when inactivating spores of Bacillus atrophaeus. These results show the potential of this material for replacing Al in thermite compositions that generate iodine for the mitigation of bacteria.

Chapter 3: Development of Experimental Setup

3.1 Introduction

Previously, a laser ignition setup had been constructed to conduct experiments with combustible mixtures for gas generation, see Figure 3.1. The purpose of those experiments was to investigate combustion characteristics and mechanisms of the mixtures as well as to analyze the released gases. Examples of the studied mixtures include:

- Sodium chlorate with various additives for oxygen generation [25].
- Ammonia borane with various additives for hydrogen generation [26].

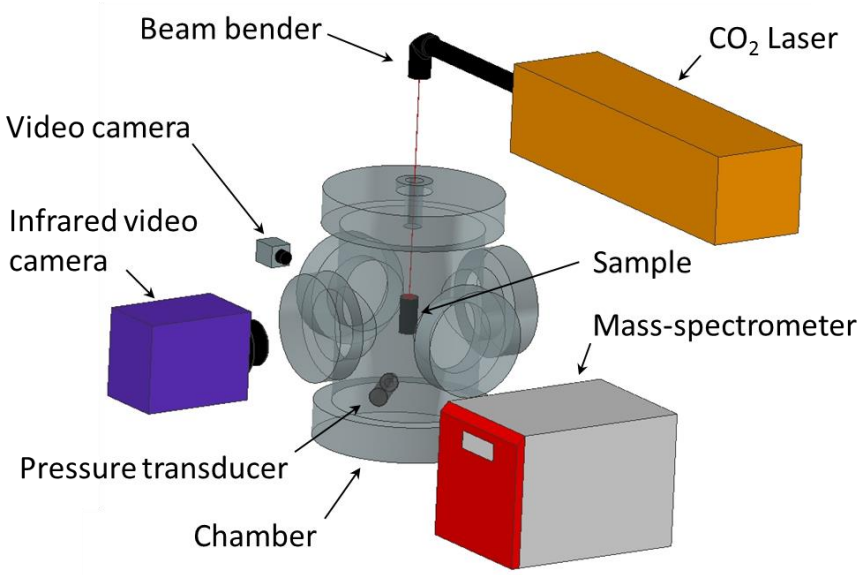

Figure 3.1: Previous experimental setup

Gas-generating mixtures can be categorized into two types:

A. Mixtures that release substances that remain gaseous under standard conditions (25°C, 1 atm) such as oxygen and hydrogen;

B. Mixtures that release substances that are gases at the combustion temperature but solid under standard conditions (e.g., iodine).

The mixtures studied in the present work are confined into the second group; the gas products return to their solid state as the testing environment comes back to standard conditions after combustion. Since the previous laser ignition setup consisted of a configuration in which only mixtures of the first group could

be tested, a new setup configuration was designed, which allowed for the condensed products to be collected and stored after combustion for analysis and characterization.

3.2 Design objectives

As previously mentioned, one of the objectives of the present work was to analyze the products of the combustion of iodine-rich thermites and quantify the iodine found in the products. Its quantification through chemical analysis required for the products of the combustion be collected after every experiment. For this reason, a combustion chamber was designed which could be easily accessible for placement of samples and removal of combustion products but remained safe and capable of containing highly exothermic reactions in the thermite samples once ignited with the laser. To ensure that the combustion chamber would remain safe and not failed under test conditions, a design failure analysis was performed on the chamber and its components; this analysis is presented in a coming section. Along with the design of a combustion chamber, electrical additions and changes were made to the available experimental setup in order to achieve a more adequate test configuration for studying the combustion characteristics and mechanisms of iodine-rich thermites. Safety additions and modifications were also performed on the experimental setup to minimize the possibility of an accident and to increase the safety of use. More on this configuration will be presented in the following sections.

The combustion chamber should be easily accessible for introduction of thermite samples and collection of combustion products; this would facilitate a faster testing iteration. It should also have the window ports for visual observation and video recording along with a window port through which the laser beam would be introduced to ignite the sample. It should also include a stable pedestal for sample placement under the window for laser beam introduction. The chamber should also be able to contain combustion gases from exiting unto the surroundings.

3.3 Combustion chamber

The boiling (sublimation) point of iodine is 184°C at 1 atm. Thus, quickly after release by the burning mixture, iodine gas begins to condense and solidify as the chamber cools down back to room

temperature. Since the condensation rate is high, it is virtually impossible to quantify the released iodine while it is in its gas form and it is necessary to collect and analyze solid products of the combustion. For this purpose, a combustion chamber was developed that was capable of containing condensed products after each combustion experiment, and allowed for easy collection of these products for analysis.

The chamber consisted of an aluminum cylinder (Volume 0.5L) with two window ports, one on each end of the cylinder. The length of the cylinder was 160mm and the inner diameter of the chamber was 70mm, while the outer diameter was 90mm. The cylinder had an opening on its side, through which the laser beam would be introduced, and a smaller opening on the opposite side of the cylinder, which would serve as the intrusion for the sample holder. The cylinder also had a grove, 3.25+.1mm tick and 1.90±.04mm deep, on each of its base faces where a rubber O-ring, cross-sectional diameter 2.4±.08mm in accordance with O-ring design handbooks, was placed for sealing of the chamber. The chamber cylinder is shown in Figure 3.3.1.

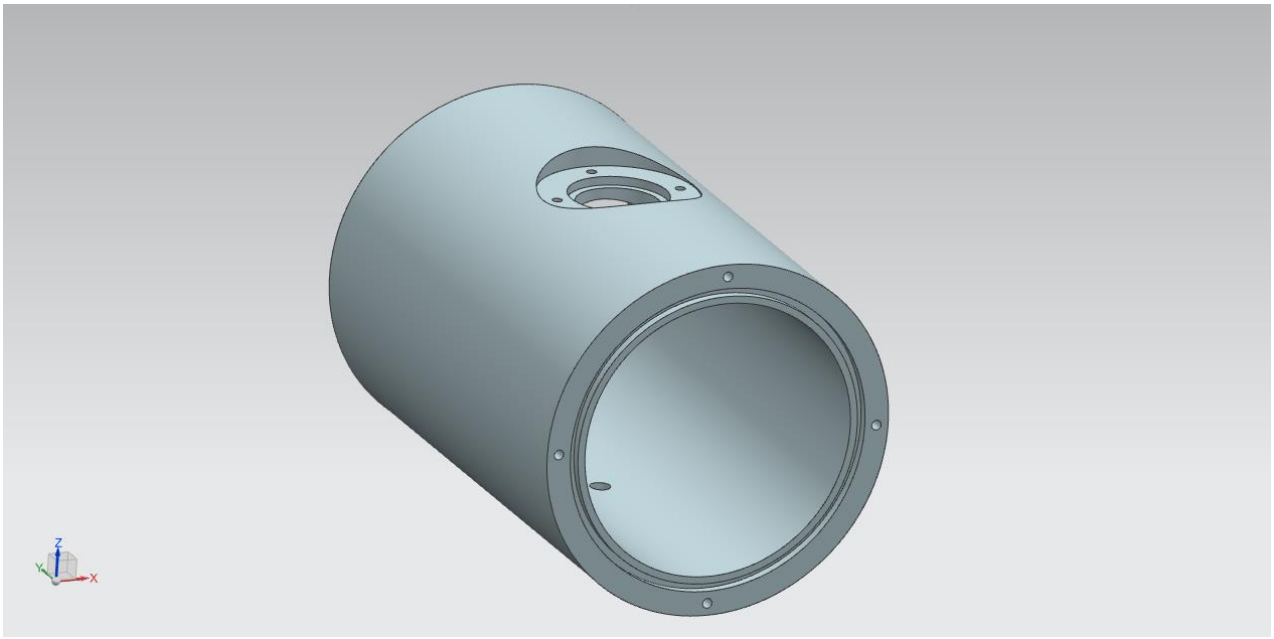

Figure 3.3.1: Main body part of the combustion chamber

Each of the window ports consisted of two aluminum pieces and one window. One of the pieces enclosed the window, while the other piece served as a lid to hold the window in place. The two aluminum pieces were sealed together with four M3 bolts. One of the windows was made of sapphire for infrared examination of the combustion, while the other was a borosilicate window for observation with a high speed camera. Both windows had a diameter of 50mm and thickness of 3mm. The windows had gaskets for sealing and protection of the windows once secured between the two aluminum pieces. The lid ports of the chamber can easily be removed by unscrewing four M3 bolts on the lid, this facilitates the collection of the combustion products. Figure 3.3.2 shows one lid of the chamber.

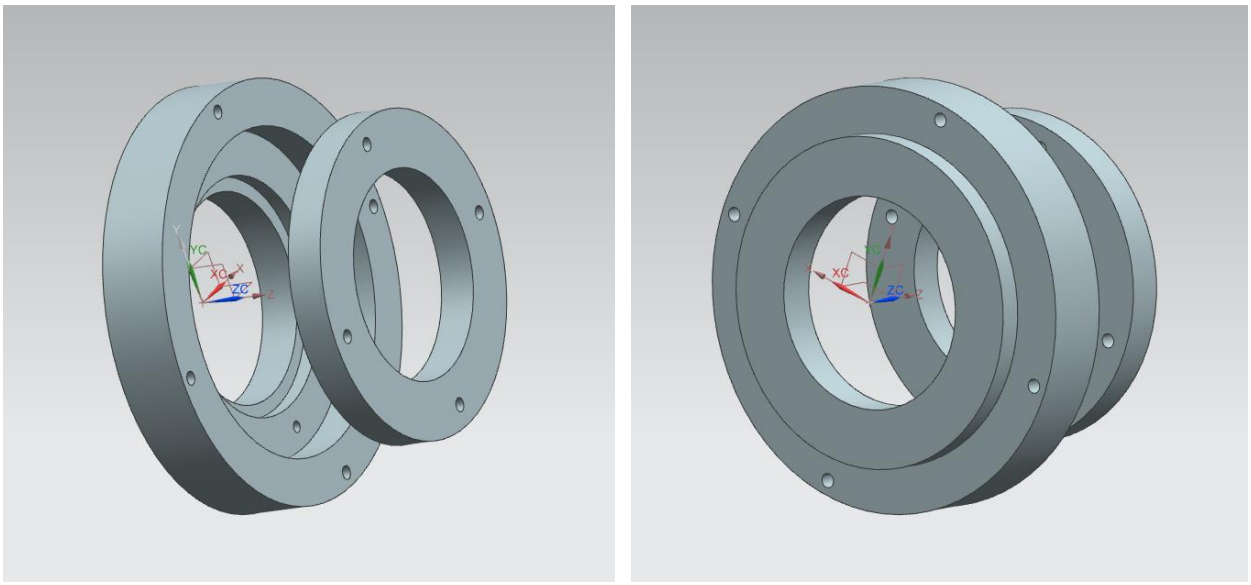

Figure 3.3.2: Outside (left) and inside (right) views of the chamber lids

The chamber had an aluminum tube extension on the lateral surface of the cylinder; at the end of this extension is a ZnSe window through which the laser enters the chamber to ignite the sample. The extension is to protect the ZnSe window from the high temperatures of the combustion and from the jet of products released as the combustion occurs. Figure 3.3.3 shows the tube extension.

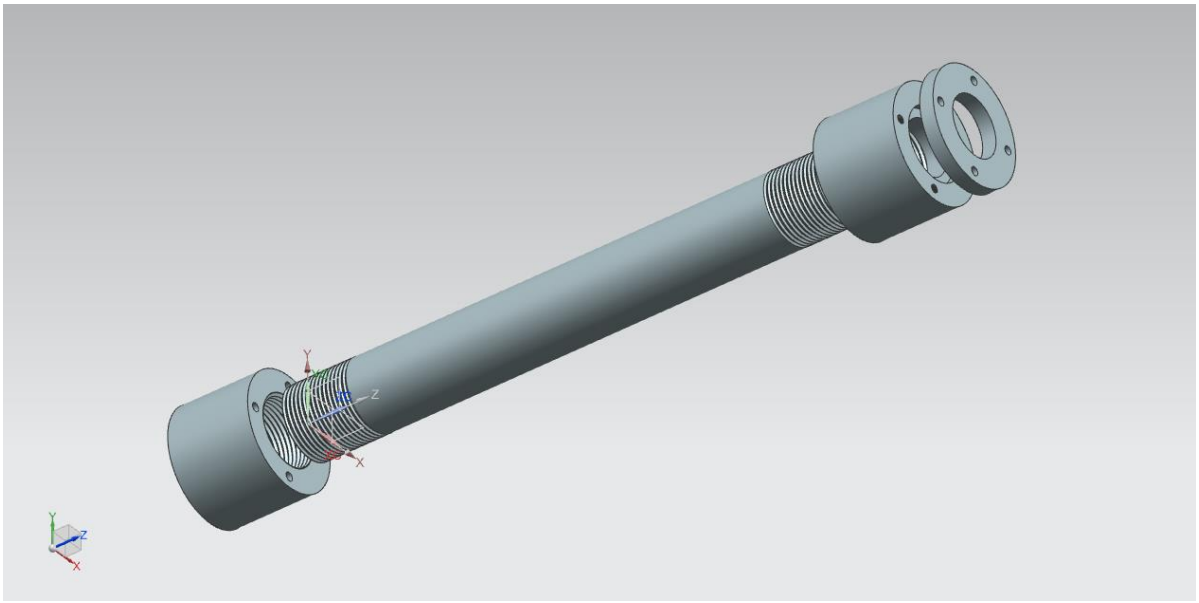

Figure 3.3.3: Chamber tube extension for laser introduction and ZnSe glass protection

A brass sample holder was also designed and fabricated to be placed inside the chamber directly under the ZnSe window in order for the laser to hit the sample. The sample holder consisted of two pieces, the first one would screw into the interior of the cylinder and would have a circular intrusion on its top where the second piece would assembled. Having one piece fixed on the chamber and the other removable would facilitate the placement of thermite samples into the chamber. Finally, a base for the chamber was fabricated, this base would allow for a stable place for the chamber to rest during an experiment. Figure 3.3.4 shows both the sample holder and base fabricated for the chamber.

Figure 3.3.4: Combustion chamber base (left) and thermite sample holder (right)

3.4 Design safety calculations

Analytical failure studies were conducted on the combustion chamber. The purpose for these studies was to be certain that no failure could occur on the chamber components during a combustion experiment, any failure could cause harm to the operator and people in the vicinity. The chamber components analyzed in this study are as follows, the borosilicate view window port, the small ZnSe window through which the laser beam is introduced to ignite samples, and lastly the bolts that hold the lids to the chamber. The main reason for components failure in the chamber would be the pressure increment that is experienced inside the chamber as the products undergo expansion during combustion. Figure 3.4 shows the combustion chamber.

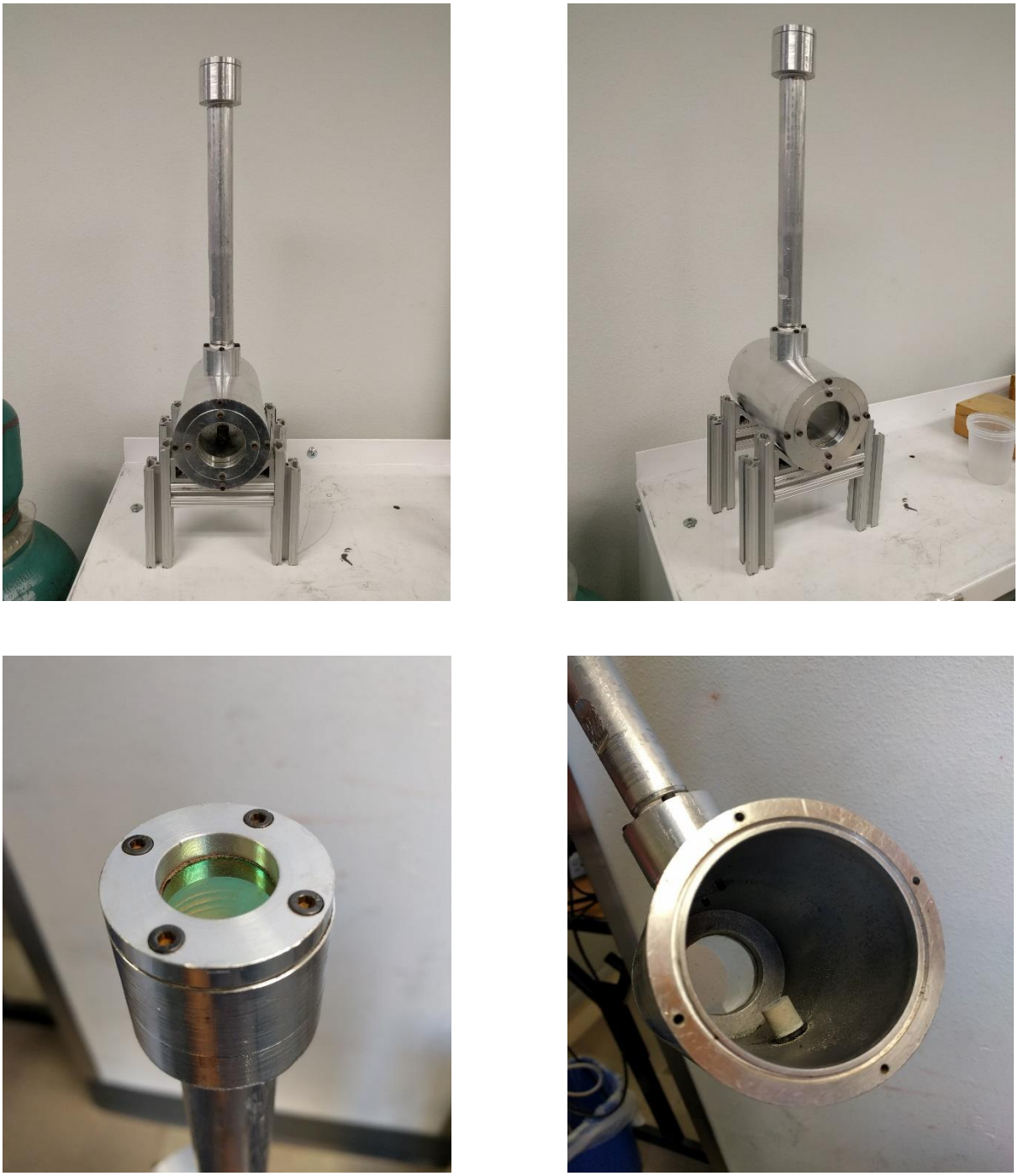

Figure 3.4: Combustion chamber on base (top). Combustion chamber ZnSe window port (bottom-left) and chamber interior (bottom-right)

It was important to also establish the amount of mass per sample that should be allowed for use in combustion experiments in this chamber. During combustion of a mixture sample, pressure in the chamber increases because of two factors: (1) the increase in the mass of gas inside the chamber due to gas generation by the mixture and (2) the increase in the temperature of the gas inside the chamber caused by combustion heat release. The increase in the mass of gas is temporary because the released gas is quickly condensed to solid state. Also, the gas mixture inside is cooled owing to heat losses to the chamber walls. Calculations, however, are conducted for the peak pressure, i.e., assuming that there is no condensation and neglecting any heat losses.

3.4.1 Maximum allowed mass of sample for iodine-containing mixtures

The constraint for the gage pressure in the chamber is 10 psig (standard safety value for non-high pressure chambers). All experiments are conducted in an air environment at atmospheric pressure. The mass of gas that, being added to the air in the chamber, will increase pressure to 10 psig, is calculated using the ideal gas equation:

$$m_{gas} = \frac{M_{gas}V}{R_u T}\Delta P \qquad (3.\ 1)$$

where M_{gas} is the molar mass of the evolved gas (e.g., 254 kg/kmol for I_2), V is the volume of the chamber (0.5 L), R_u is the universal gas constant (8.314 kJ·kmol^{-1}·K^{-1}), T is the gas temperature, and ΔP is the allowed gage pressure (10 psig = 68.9 kPa).

The mixture typically includes a compound (e.g., Al·I_2) that is a source of the gas and the additive (e.g., Fe_2O_3) that reacts with the gas source leading to the gas release. If the mass of the gas is known, the mass of the gas-containing compound (e.g. Al-I_2) is determined from:

$$m_{comp} = \frac{m_{gas}}{mf_{gas}} \qquad (3.\ 2)$$

where m_{gas} is the mass of the gas and mf_{gas} is the mass fraction of the gas in the compound. The mass of the sample (e.g. Al-I_2/Fe_2O_3) can then be calculated as:

$$m_s = \frac{m_{comp}}{mf_{comp}} \qquad (3.3)$$

where mf_{comp} is the mass fraction of the gas source in the mixture sample.

The concentration of the additive corresponds to the stoichiometry of the reaction between the source of gas and the additive (the amount of gas per unit mass of the mixture is less than in the first case, but the temperature is high). For example, the stoichiometric reaction between Al-I_2 (20 wt% I_2) and Fe_2O_3 is described by the following equation:

$$2\ Al + 0.5(M_{Al}/M_{I2})\ I_2 + Fe_2O_3 \rightarrow 2\ Fe + Al_2O_3 + 0.5(M_{Al}/M_{I2})\ I_2 \qquad (3.4)$$

where M_{Al} and M_{I2} are the molar masses of Al and I_2, respectively. The gas temperature is calculated from the energy balance:

$$T = \frac{c_{v,gas} m_{gas} T_{ad} + c_{v,air} m_{air} T_o}{c_{v,gas} m_{gas} + c_{v,air} m_{air}} \qquad (3.5)$$

where T_o is room temperature, $c_{v,gas}$ and $c_{v,air}$ are the specific heats of the gas and air, respectively at constant volume (e.g., 0.13 kJ·kg^{-1}·K^{-1} for I_2 and 0.72 kJ·kg^{-1}·K^{-1} for air), T_{ad} is the adiabatic flame temperature for the mixture at 1 atm, calculated using THERMO (version 4.3) software, available in the laboratory (e.g., 3052 K for Equation 3.5), and m_{air} is the mass of air in the chamber, calculated using the ideal gas equation:

$$m_{air} = \frac{P_a V}{R T_o} \qquad (3.6)$$

where P_a is atmospheric pressure (assumed to be 90 kPa in the laboratory) and R is the gas constant of air (0.287 kJ·kg^{-1}·K^{-1}).

First, T_{ad} is calculated using THERMO and the mass of air is calculated from Equation 3.6. Then the mass of gas is calculated using Equation 3.1 assuming that $T=T_o$. Then temperature is calculated from Equation 3.5. Then the next iteration is conducted for Equation 3.1, and so on, until the temperature difference in two subsequent iterations becomes less than 1 K. Such calculations were conducted for all iodine-containing mixtures studied in this paper, and the final iteration resultant masses are presented in

Table 3.4. These results serve as limit of sample mass that should not be exceeding for each respective mixture in order to not increase the pressure inside the chamber by 10 psig (68.9 kPa).

Table 3.4: Sample mass which increases the pressure in the chamber by 10 psig (68.9 kPa)

	Al-I_2/Fe_2O_3	**Al-I_2/Bi_2O_3**	**Al-I_2/MoO_3**	**Al-I_2/CuO**	**Al-I_2/I_2O_5**
I_2 mass (g.)	1.089	1.056	0.984	1.133	0.064
Al mass (g.)	4.356	4.226	3.934	4.531	0.256
Oxide mass (g.)	12.91	36.54	9.325	20.14	1.18
Sample mass (g.)	18.35	41.83	14.24	25.80	1.49

3.4.2 Viewing window port

The chamber has two window ports for observation. One of the view window ports is a sapphire window used for observation with an infrared camera. The other window port is made of borosilicate and is used for observation with a high speed camera. According to the Introduction to Materials Science for Engineers by J. Shackelford, sapphire and borosilicate have modulus of rupture (MOR) of 350 MPa and 69 MPa, respectively, i.e. borosilicate had the lowest mechanical strength. Since these two windows have the same diameter and thickness, the borosilicate window would suffer failure first. The failure study was then performed on the borosilicate window. A factor of safety of 2 was used in this study; therefore the stress limit for the Borosilicate window was fixed at 34.5 MPa. A representation of this window and the stresses it experiences are shown in Figure 3.4.1.

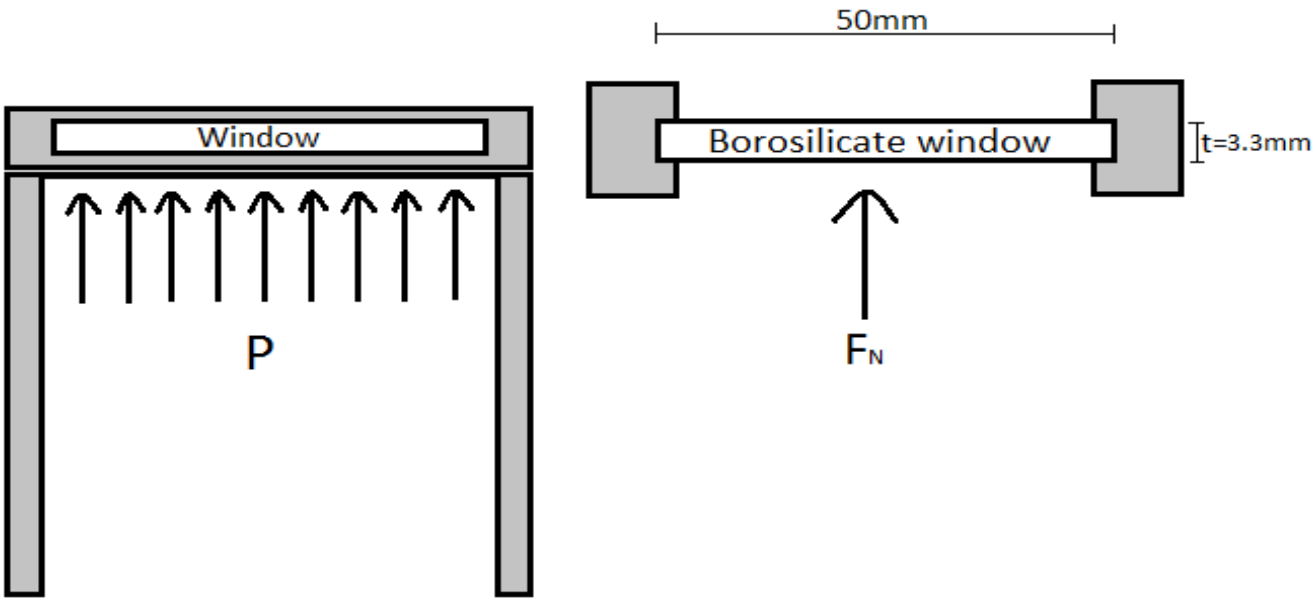

Figure 3.4.1: Borosilicate window representation with experienced pressure

In order to determine the pressure P at which the window would fail, the assigned borosilicate stress limit was set as the stress experienced by the window (σ_w =34.5 MPa), σ_w was then multiplied by the window area over which the stress is experienced to obtain the load normal to the window (F_N), this area is equal to the circumference (c =.157 m) of the window times its thickness (t=.0033 m). This calculation and the resultant F_N are shown below:

$$F_N = \sigma_w * (t * c),\ F_N = 17.87\ kN \tag{3.7}$$

Next, F_N was divided by the face area of the window (Aw =.00196 m^2) to find the pressure P over the window inside the chamber, the calculation and resultant P are shown below:

$$P = \frac{F_N}{A_w},\ P = 9.12\ MPa \tag{3.8}$$

Thus, the borosilicate window will fail if the pressure inside the chamber exceeds 9.12 MPa.

3.4.3 Laser window port

For the case of the ZnSe window, the Knoop hardness is 120 $kg_f \cdot mm^2$ (17 GPa).Thus, for a factor of safety of 2, the stress limit is 588.4 MPa. The same failure study approach as with the borosilicate window was taken. A representation of this case is shown in Figure 3.4.2. The assigned stress limit was set as the stress experienced by the window (σ_w), then this stress was multiplied by the area over which it is exerted on the window to find the load normal to the window (F_N), this area as in the previous case was found by multiplying the window's circumference (c =.078 m) times its thickness (t =.0033 m). This calculation and the resultant F_N are shown below:

$$F_N = \sigma_w * (t * c),\ F_N = 151.45\ kN \tag{3.9}$$

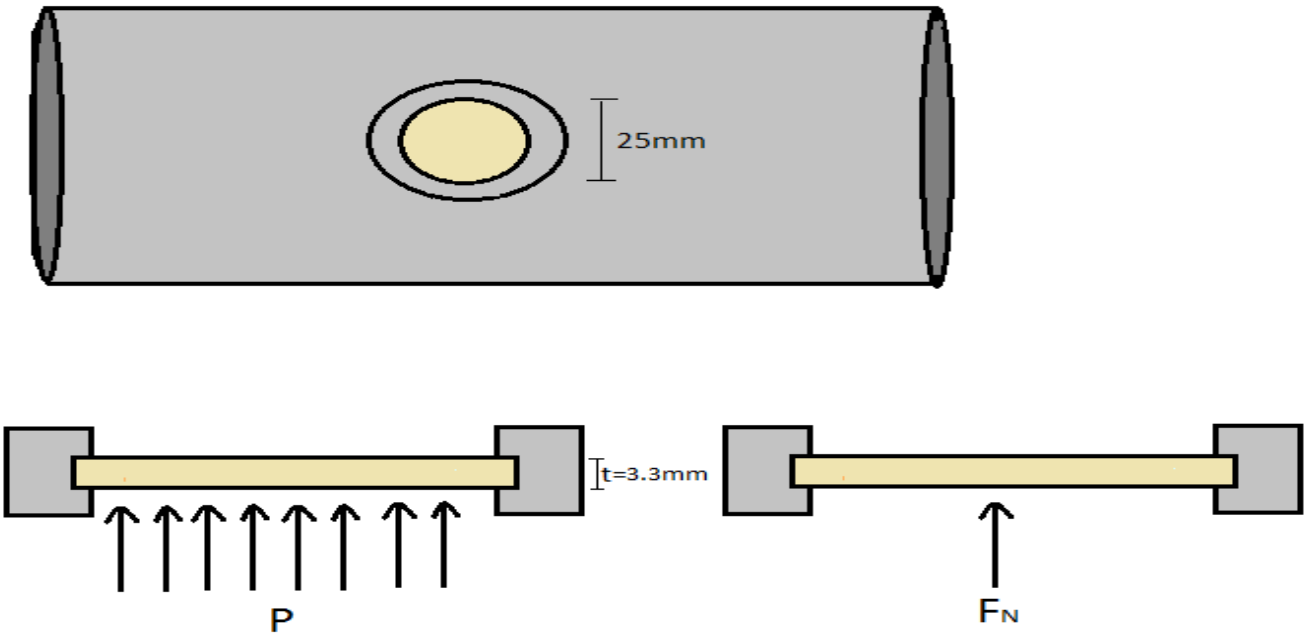

Figure 3.4.2: Borosilicate window representation with experienced pressure

Next, F_N was divided by the face area of the window (A_w =.00038 m_2) to find the pressure P over the window inside the chamber, the calculation and resultant P are shown below:

$$P = \frac{F_N}{A_w},\ P = 398.4\ MPa \tag{3.10}$$

Thus, the ZnSe window will fail if the pressure inside the chamber exceeds 398.4 MPa.

3.4.4 Chamber lids bolts

Stainless steel M3x.5 bolts are used to attach the top and bottom lids to the chamber and sealed it off so that no combustion products can escape the inside of the chamber. In total, 8 bolts are used to enclose the chamber, 4 bolts per lid.

In order to determine what the pressure inside the chamber has to be for the bolts to fail, first the proof load for the bolts had to be established. The proof load for a bolt is 75% of the tensile strength of the bolt material, bolts were made of carbon-steel and its tensile strength is 240 MPa. If the stress experienced on a single bolt exceeds the proof load, then failure would happen in the bolt. The pitch diameter for M3x.5 bolts is D_p = 2.53mm and its minor diameter is D_m= 2.272mm. Figure 3.4.3 shows a representation of the bolts in the chamber and the load they experience.

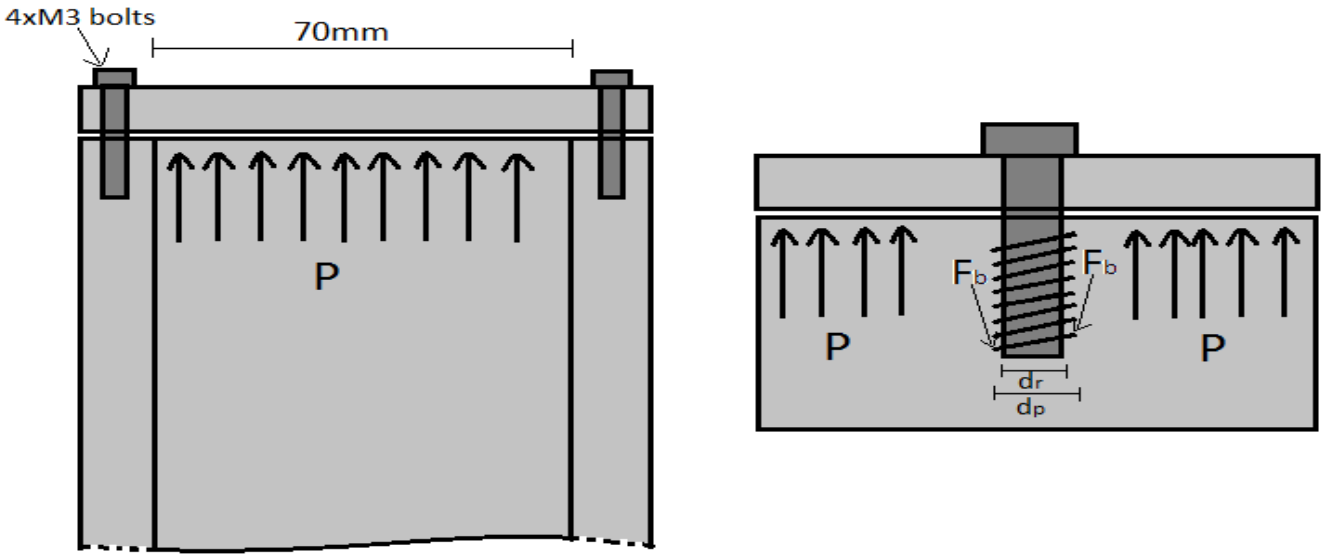

Figure 3.4.3: Diagram representing the bolts on chamber and the forces on them

To find the pressure inside the chamber (P) that would cause the bolts to fail, the bolt proof load was set as the stress experienced on a bolt (σ_b), next the σ_b was multiplied by the 'tensile stress area of the bolt' to determine the load on the bolt (F_b), the tensile stress area was obtained using the minor and pitch diameter of the bolt. These calculation and the resultant F_b are shown below:

$$F_b = \sigma_b * \frac{\pi}{16}\left(D_p + D_m\right)^2,\ F_b = 814.3\ N \tag{3.11}$$

Then F_b was multiplied by 4 to account for all the bolts in one lid and obtain the load exerted normal to the lid (F_L), this load was calculated to be 766 N. Finally, pressure P inside the chamber was calculated by dividing F_L by the internal face area of the lid (A_L =.00385 m^2). Calculations for P and its resultant are shown below:

$$P = \frac{F_L}{A_L},\ P = 857.1\ kPa \tag{3.12}$$

The pressure P inside the chamber that will cause the bolts to fail was found to be 857.1 kPa.

3.4.5 Conclusion

The mechanical failure study has shown that the lid bolts will be the first elements of the chamber to fail. According to the calculations, the maximum pressure allowed is 857 kPa. This is significantly higher than the maximum allowed safe pressure of 69 kPa (10 psig). Thus, the chamber will not fail provided the sample mass does not exceed the calculated maximum allowed mass.

3.5 Electrical design

In the available experimental setup, the CO_2 laser is powered by a 48+ VDC power supply (Mean Well), connected to a 208 VAC outlet. To control and monitor the power of the laser beam, a unit controller (Synrad UC-2000) was utilized. Using the controller, the laser beam power can be regulated. To power this controller, a 5VDC power supply was used. This controller was also set in communication

with a computer through a solid state relay. In the computer, the controller's input and output were added to and managed by LabView software. In LabView, a program was created to give the ability to control the lasing time of the laser, therefore a desired time, e.g. 3seconds, could be inputted. Clicking on the run button LabView would send a 3 second pulse to the controller which in turn would send the signal to the laser to turn on and lase for 3 seconds and then stop. Lasing could also be stopped at any point directly from the LabView program in the computer.

Since new testing capacities were required for the work presented in this paper, additions to the electrical setup configuration described above were needed. An important requirement when determining the point of ignition and self-propagation of a thermite sample when using the laser is to know the laser would only help ignite the sample but not contribute to the combustion propagation over the sample. Ideally, the laser would need to stop lasing as soon as ignition was reached in order to be sure that the combustion was self-propagating. In the laser-electrical configuration previously described, it was unknown if the laser was contributing to the combustion of the sample as the laser would work for the assigned amount of time. For example, if the laser was set to work for 2 seconds but ignition happened after 0.8 seconds of heating by the laser, then the laser would continue to assist the combustion of the sample. Lasing could be stopped from the computer once it was observed that ignition happened but the ignition and combustion times of the samples studied in this work are too short making it improbable for accurately stopping the laser at the time of ignition. Because of this, an addition to the setup was made with which the laser could be stopped immediately after sample ignition. To accomplish this a photo-resistor was used at one of the window ports of the combustion chamber. This photo-resistor would signal when ignition had occurred and the laser would then be shut off. In the sections below the configuration and function of this addition will be covered.

As a precaution measure, a revolving light turret was added to the setup, so the light would turn on every time the laser would be in the lasing regime during an experiment. This was done with the aim of letting people in the surroundings know when the laser was being used. Also to make the experimental setup and the use of the laser safer and more secure, an emergency stop switch was added. Tthe

configuration and function of these additions are described below. A connection diagram of this is shown in Figure 3.5.

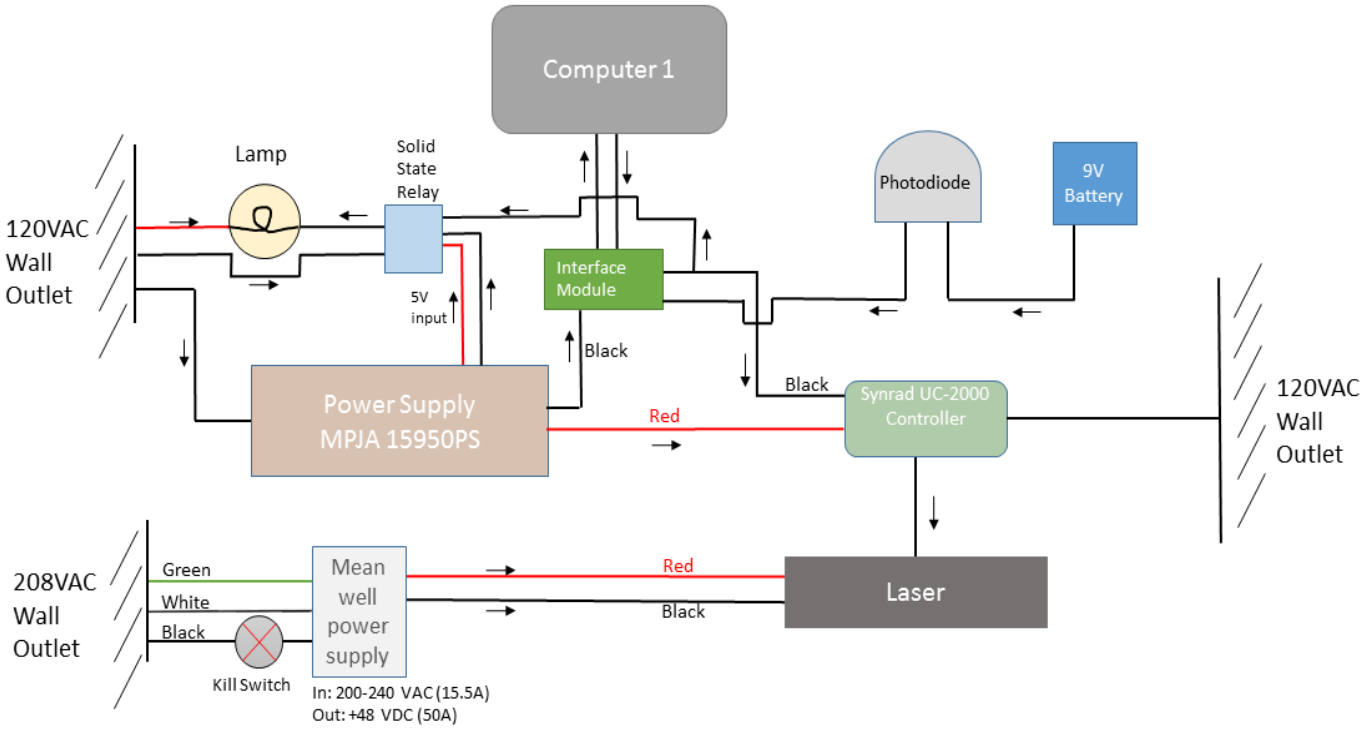

Figure 3.5: Electrical connections diagram for experimental setup

3.5.1: Photo-resistor laser stoppage

The need to stop the laser from assisting the combustion of samples during an experiment was met with the addition of a setup which consisted of a 50kOhm (dark resistance value) photo-resistor, a 9V battery, a 10kOhm resistance, an interface module between photo-resistor and a computer with LabView software. When the thermite samples are ignited with the laser, the ignition creates a bright light which then is caught by the photo-resistor placed on a window of the chamber, Figure 3.5.1 shows the photo-resistor placement. The photo-resistor reduces its resistance allowing for voltage coming from the battery to flow through. This voltage is then received by the interface module which in turn sends the signal to the Labview program to stop the laser.

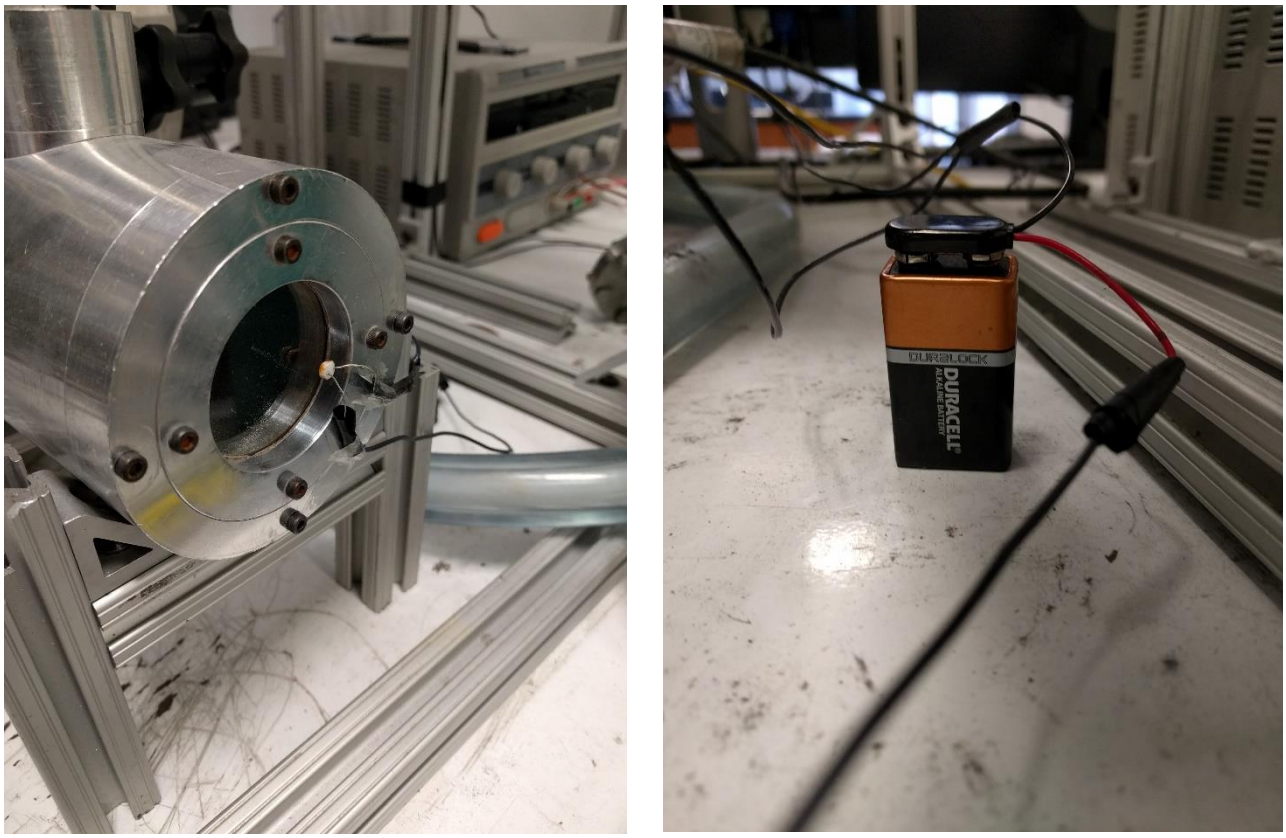

Figure 3.5.1: Photo-resistor placement on chamber (left) and battery for photo-resistor (right)

In the LabView software, when acquiring data or a signal from an external source, e.g., a photo-resistor, two types of inputs are read by the software, input high and input low which can be referred to as True signal or False signal respectively. For an input high to be read, the voltage coming in had to be 5.5V or higher, anything else would be read as input low. Therefore a battery of 9V was used so that when the photo-resistor would caught light and its resistance dropped, a voltage of approximately 6.3V would flow to the interface module and then read in the Labview program as an input high which would in turn stop the laser. The 10kOhm resistor serves both as a voltage divider and reference point to measure voltage changes. Below in Figure 3.5.2 a connection diagram of the photo-resistor is shown.

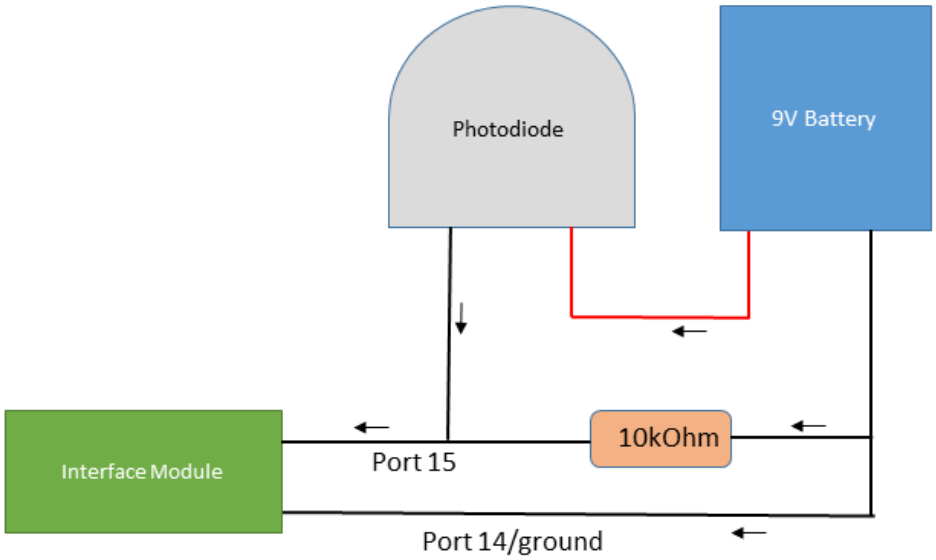

Figure 3.5.2: Diagram of electrical connection for the photo-resistor

As stated above, a LabView software program had to be developed in order to have control over the laser. It was explained earlier in this section that previously a program had been developed which allowed the assigning of time the laser would turn on and lase. This program also provided a button with which the lasing could be stopped at any time. Because of the addition of a photo-resistor to more accurately stop the laser at time of ignition, the program needed to be re-made and the logic behind it became more complex than it was in the previous program as the laser was no longer simply ruled by a timer and stop button but also by an input signal coming from the photo-resistor which would override the other commands. Figure 3.5.3 shows images of both the user interface of the program and the logic program interface.

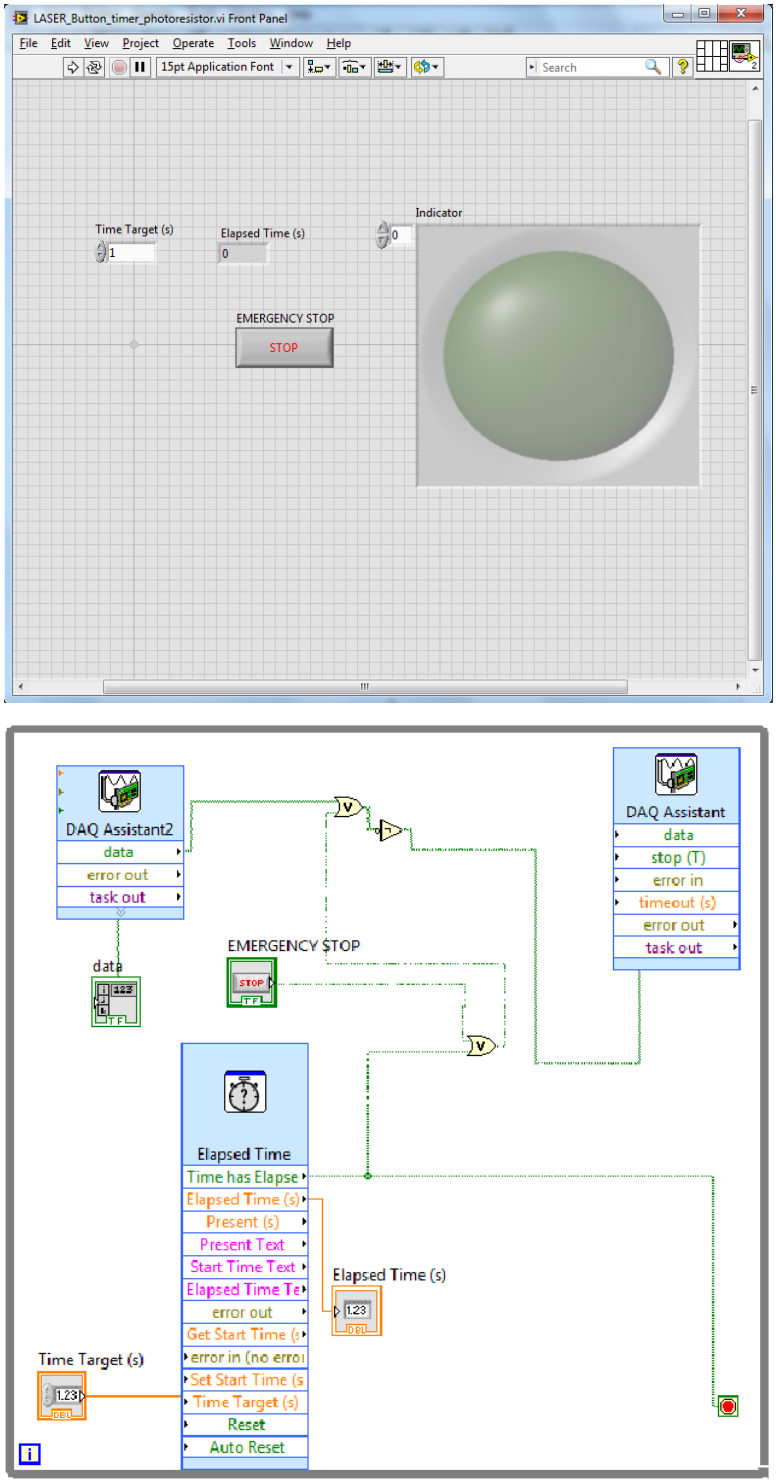

Figure 3.5.3: Laser LabView program user interface (top), and logic schematic for program (bottom)

For a reader's better understanding of the program developed, the program was divided into two parts. The first part encompasses the timer used for assigning a lasing time and the stop button for the laser, while the second part encompasses the output from the first part and the input received from the photo-resistor. It is important to acknowledge that the LabView software logic is based on positive Trues (T) and negative Falses (F) signals. It was found that the final output of the program needed to be a False (F) in order for LabView to send the signal to stop the laser, therefore this was the end goal of the logic developed for this program. A diagram for part one is shown in Figure 3.5.4 and the logic and outputs are shown in Table 3.5.1.

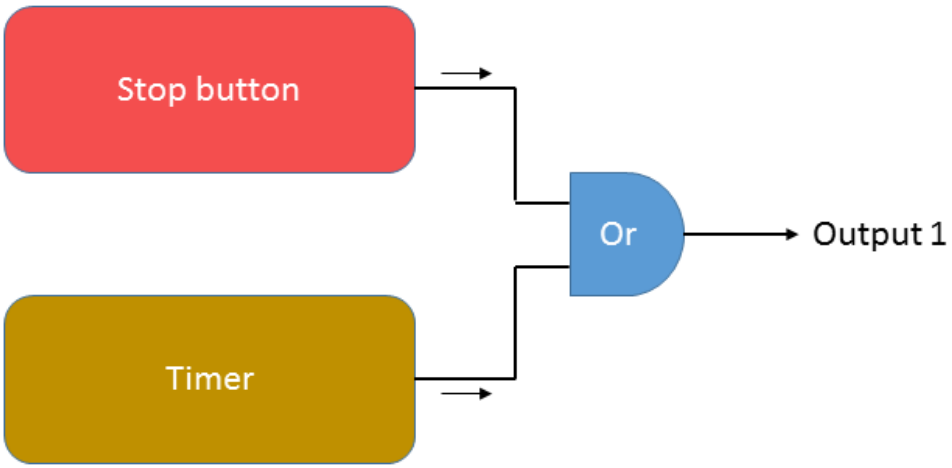

Figure 3.5.4: Logic schematic for part one of the laser program

Table 3.5.1: Logic table for laser program part one

Part 1 Logic Table - OR function		
Timer	**Stop Button**	**Output 1**
T	T	T
T	F	T
F	T	T
F	F	F

Timer
T = Time ended
F = Time running

Stop Button
T = Pressed
F = Unpressed

For the first part of the program, a timer was again included which could be used to set an amount of time for lasing. As shown in Table 3.5.1, when the timer is running, the output it provides is a False (F) and when the assigned time has run out, it provides an output of True (T). The second element of the first part of the program was the stop button which could be used to stop the lasing at any point desired. When the button was un-pressed, the output produced would be a False (F), whereas when the button was pressed, it would produce an output of True (T). The outputs produced by both the timer and the stop button enter an OR function from Labview. This function looks at the inputs of the timer and stop button together and if any of them is a True (T), it produces a True (T) output as well, this output is called Output 1 for better understanding and alignment with the diagrams. If the timer were to be running and therefore the laser was lasing and the stop button was pressed, this would give out an output of False (F) for the timer but a True (T) for the stop button; therefore Output 1 would produce an output of True (T). But in the case that both outputs from the timer and stop button were False (F), that is time was still running in the timer and the stop bottom had not been pressed, then the OR function would produce a False (F) Output. This logic is presented in Table 3.5.1. The output produced by the OR function, Output 1, is then used in part Two of the program. The diagram for part Two is shown in Figure 3.5.5, and the logic and outputs are shown in Table 3.5.2.

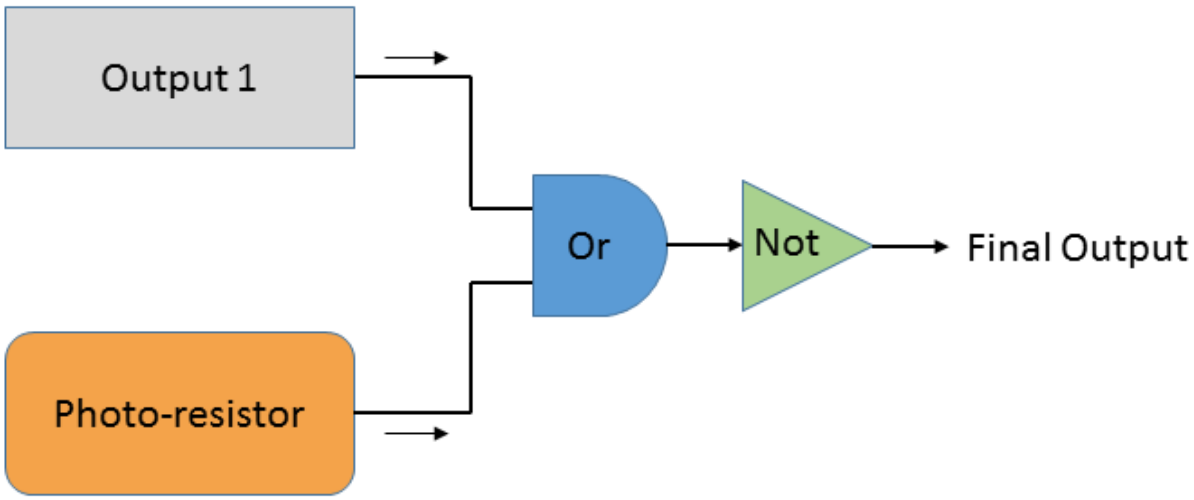

Figure 3.5.5: Logic schematic for laser program part two

Table 3.5.2: Logic table for laser program part two

Part 2 Logic Table - OR & NOT functions		
Output 1	**Photo-Resistor**	**Final Output**
T	T	F
T	F	F
F	T	F
F	F	T

Photo-resistor
T = Ignition
F = No ignition

For the second part of the program, the output from the first part is used along with the output produced by the incoming signal of the photo-resistor. As seen above, when no ignition has been achieved, the output produced by the photo-resistor is a False (F), whereas if ignition has been reached in the chamber, the photo-resistor would produce an output of True (T). Again a function OR was used to read the outputs of both the first part of the program and the photo-resistor. This, as explained before, would produce a True (T) output if either the photo-resistor or Output 1 produced a True (T) and would only produce a False (F) when both the photo-resistor and Output 1 were to produce a False (F). But as stated earlier in this section, LabView requires a False (F) signal to be produced in order to shut down the laser. Therefore, a NOT function was added after the OR function, this would flip Trues (T) to Falses (F) and Falses (F) to Trues (T). This then would made the Final Output False (F) if either the photo-resistor or Output 1 produced a True (T), and would made the Final Output True (T) only if both the photo-resistor and Output 1 were to produce a False (F). In the case when a False (F) was produced from Output 1, meaning that neither the timer has finish running nor the stop button has been pressed, and also a False (F) was produced by the photo-resistor, then a True (T) would be the Final Output and the laser would continue to lase. The lasing would continue until either the time runs out, the stop button is pressed, or ignition is read by the photo-resistor; either of these cases would produce a True (T) output which in turn would generate a False (F) for the Final Output which is required to stop the laser.

3.5.2 Relay and signaling light

When the infrared (invisible) beam is being generated by the laser, i.e. the lasing takes place, the LEDs on the laser indicate this event and a specific sound is emitted by the laser. As an additional warning measure, a 120 VAC red incandescent revolving light, Tri Lite MVLP, shown in Figure 3.5.6, is used to alert the operator and those in the surroundings of when the laser beam was being generated. Since the light had a magnetic bottom, a steel plate was fasten to the top of the setup and the light was then placed on the top of this plate. It turns on when lasing begins and turns off when the lasing stops.

Figure 3.5.6: Laser in-use revolving incandescent light

To control the current flow into the light, a SainSmart 5 V 2-channel solid state relay board, shown in Figure 3.5.7, was used. One contact of the light was connected to a 120 VAC outlet, while the other contact was connected to the inlet port of the SSRB, see Figure 3.5. The outlet port of the SSRB was connected to the 120 VAC outlet. The SSRB was powered with the same 5 VDC power supply that powered the Synrad UC-2000 controller in the laser setup. The SSRB was also connected to the wire that connects the Computer and the Synrad UC-2000 controller, this wire transmitted the lasing on/off signals from LabView to the controller.

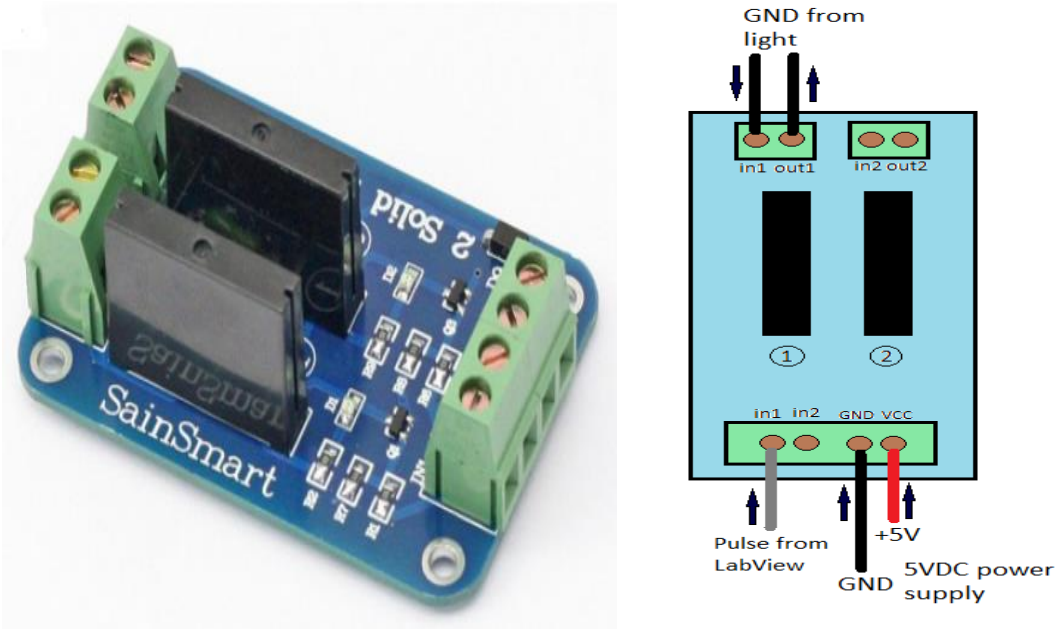

Figure 3.5.7: SainSmart 5 V 2-channel solid state relay board

3.5.3 Laser emergency power shutdown

In the occasion where the laser has to be turned off at once, the operator will not have to reach the computer to stop the laser. The operator or anyone in the vicinity can easily press the e-stop switch nob. This will cutoff current to the Mean Well power supply so that the laser will be immediately shut down. After resolving the emergency situation, the current to the power supply can be restored by turning the e-stop switch nob clockwise to release it; this will allow current to flow to the power supply again.

The emergency kill switch as shown in Figure 3.5.8 was connected to the ground cable of the Mean Well power supply, the ground cable coming from the 208 VAC outlet was connected into the Normally Closed (NC) port of the kill switch, while the ground cable coming from the power supply was connected to the other side of the kill switch on its Common port. In this configuration, the power would commonly be flowing to the power supply as the Normally Closed port was used and in the case of an emergency, when the button of the switch was pressed, the circuit would be opened, therefore cutting the power to the power supply and in turn the power to the laser.

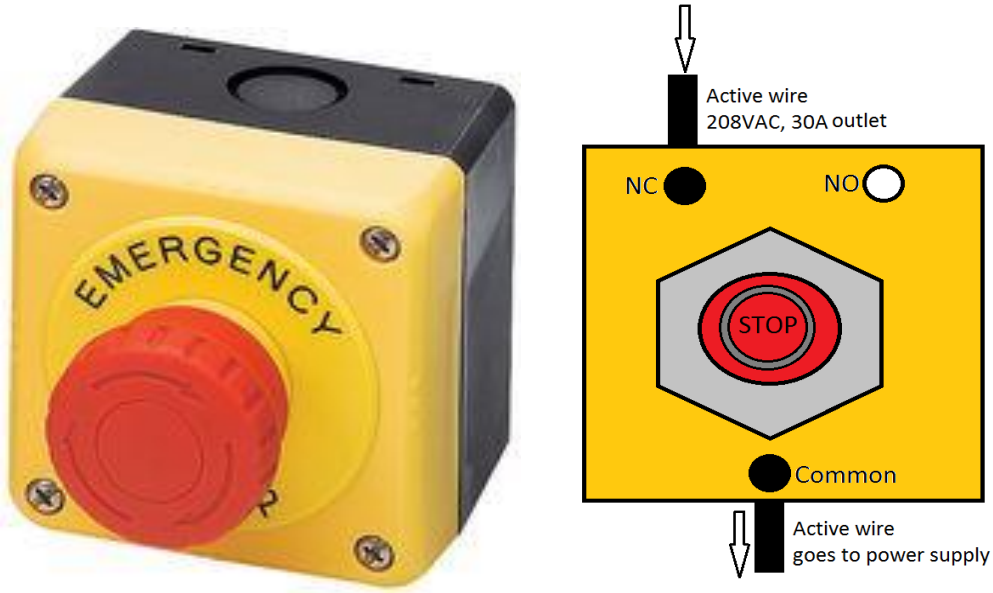

Figure 3.5.8: Normally closed emergency kill switch

3.6 Summary

A previous setup allowed only for the investigation of mixtures which generate products such as oxygen and hydrogen that remain in gaseous form after combustion. In the presented work, the released products (iodine) are in gaseous form at combustion temperatures but rapidly condense as the environment returns to standard conditions. To study combustion of these mixtures, the development of a new experimental setup was required.

A chamber was designed and built to accommodate for the testing of iodine-containing mixtures. The requirements for this chamber include: accessibility for sample placement and product collection, ability for visual observation of combustion, accessibility of laser for sample ignition, and capability to safely contain combustion temperatures and pressure increments. Chamber was designed and built of aluminum. It contained two window ports, one (borosilicate glass) for high speed video recording and the other one (sapphire) for infra-red camera recording. A zinc selenide window was used for laser introduction and an aluminum tube extension was added to protect this window from the high-temperature combustion products.

The maximum allowable sample mass was determined for each mixture. During combustion, the generation of high-temperature gases increases pressure in the chamber. Although pressure quickly decreases because of iodine condensation and heat losses to the walls, it is important not to create even a short pulse of high pressure. Thermodynamic calculations were performed in order to determine the sample allowed mass for a pressure increment of 69 kPa (10 psig), which is a standard upper limit for low-pressure vessels.

A failure study was performed on three components of the chamber: viewing window ports, laser window port, and chamber lid bolts. A factor of safety of two was used in the calculations. The chamber lid bolts were found to be the components to first become structurally compromised, with the maximum allowed pressure inside the chamber being by an order of magnitude higher than 69 kPa, upper pressure limit used in allowable sample mass study. This guarantees structural integrity of the chamber during the experiments.

Electrical modifications and additions were performed to the experimental setup for more appropriate testing of studied mixtures. A photo-resistor was added in order to automatically stop the laser upon ignition of the sample. A LabView-based program, previously used to control the lasing time and manually stop lasing, was modified to accommodate for the addition of the photo-resistor's input. A physical emergency kill-switch was added along with a rotating red-incandescent light which alerts anyone in the surroundings when the laser beam is being generated.

Chapter 4: Experimental Procedure

4.1 Introduction

A set of thermites for combustion experiments was prepared with mechanically alloyed Al-I_2, while the other set of thermite samples was prepared with ordinary aluminum as the metal fuel. Combustion experiments were conducted with the following reactive mixtures:

- Iodine-containing metal fuel thermites: Al-I_2/Fe_2O_3, Al-I_2/CuO, Al-I_2/Bi_2O_3, Al-I_2/MoO_3, and Al-I_2/I_2O_5.
- No-iodine metal fuel thermites: Al/Fe_2O_3, Al/CuO, Al/Bi_2O_3, Al/MoO_3, and Al/I_2O_5.

The set of thermites with ordinary aluminum was prepared for comparison of their ignition and combustion mechanisms with those of the iodine-containing ones, which would help understand the effect of iodine on the combustion. All thermite mixtures prepared were compressed into cylindrical pellets and ignited using a laser for an exothermic self-sustaining combustion. After combustion of thermite samples containing iodine, a chemical analysis using titration (sodium thiosulfate as the titrant), was performed on the products collected from the chamber.

Mechanically alloyed Al-I_2 (20 wt% I_2) powder was fabricated at the New Jersey Institute of Technology using ball milling at the liquid nitrogen temperature. An attritor mill was used, with the milling chamber chilled by flowing liquid nitrogen (details are given in [10]). A commercially available aluminum powder (97.5% pure, spherical, Alfa Aesar) was used in the experiments conducted for comparison. Bismuth (III) oxide (Bi_2O_3, 99.9% pure), copper (II) oxide (CuO, >99.0% pure), and molybdenum (VI) oxide (MoO_3, 99.5% pure) were obtained from Alfa Aesar, while iron (III) oxide (Fe_2O_3, >99% pure) and iodine pentoxide (I_2O_5, 98% pure) were supplied by Sigma Aldrich.

Particle size distributions of the used powders were determined using a multi-laser particle size analyzer (Microtrac Bluewave) with isopropyl alcohol as the carrier liquid.

4.2 Sample preparation

Both Al and Al-I_2 powders were mixed with the oxides according to the stoichiometries of Al-oxide reactions (Equations 4.1 – 4.5). For Al-I_2 based compositions, the iodine was considered an inert

additive, i.e., after calculating the mass of Al powder needed for a stochiometric thermite composition, the mass of Al-I_2 powder was calculated knowing that the Al-I_2 composite powder contains 80 wt% Al.

$$2Al + Fe_2O_3 \rightarrow Al_2O_3 + 2Fe \quad (4.1)$$

$$2Al + Bi_2O_3 \rightarrow Al_2O_3 + 2Bi \quad (4.2)$$

$$2Al + MoO_3 \rightarrow Al_2O_3 + Mo \quad (4.3)$$

$$2Al + 3CuO \rightarrow Al_2O_3 + 3Cu \quad (4.4)$$

$$10Al + 3I_2O_5 \rightarrow 5Al_2O_3 + I_2 \quad (4.5)$$

Initially the mixing of the powders was conducted with a three-dimension inversion kinematics tumbler mixer (Bioengineering Inversina 2L), where the powders were dry mixed for approximately 15 minutes at high intensity rotations. After visual examination, it was observed that the products from this mixing procedure contained many material agglomerates along with large amounts of powder stuck on the walls of the container. Since a fine and uniform mixture was desired, an alternative mixing procedure was explored.

Wet mixing was performed using an acoustic mixer (Resodyne LabRam). The stoichiometric mixtures were placed in a plastic container and hexane was added in order to prevent any reaction during the mixing process. It was found that a mixing intensity of 40% for approximately 2 minutes was an adequate practice for obtaining a uniform and fine mixture. After wet mixing, the container was taken into a vacuum in a steel chamber in order to remove the hexane and dry out the mixed powders. Figure 4.2 shows images of the powders after the initial dry and latter wet mixing processes for comparison.

Figure 4.2: Dry mixed powder in Bioengineering Inversina mixer (left) and wet mixed powder in Resodyn LabRam acoustic mixer (right)

The mixed powders were then compacted into cylindrical pellet samples with the use of a trapezoidal split sleeve pressing die (composed of three sleeves) and a Carver uniaxial hydraulic press. The pressing force was equal to 19.6 kN and the time for each pellet compression was approximately 15 minutes. Pellets had a diameter of 6 mm and height of 7-14 mm. The mass was 0.8-1.4 g depending on the metal oxide content in the mixture.

4.3 Combustion experiments

The pellets were ignited by an infrared (wavelength 10.6 μm) beam of a CO_2 laser (Synrad Firestar ti-60). The experiments were conducted in air at atmospheric pressure. Figure 4.3 shows a schematic of the experimental setup. The combustion chamber consisted of aluminum cylinder (inner diameter 70 mm, length 160 mm) equipped with two removable window ports for observation and a zinc selenide (ZnSe) window along with an aluminum channel through which the laser is introduced. Details on the chamber and other components of the experimental setup can be found in the previous chapter. The pellet is

installed vertically on a brass pedestal which is then introduced into the chamber and placed under the ZnSe window. The laser beam enters the chamber through the ZnSe window and heats the top surface of the pellet until ignition is reached.

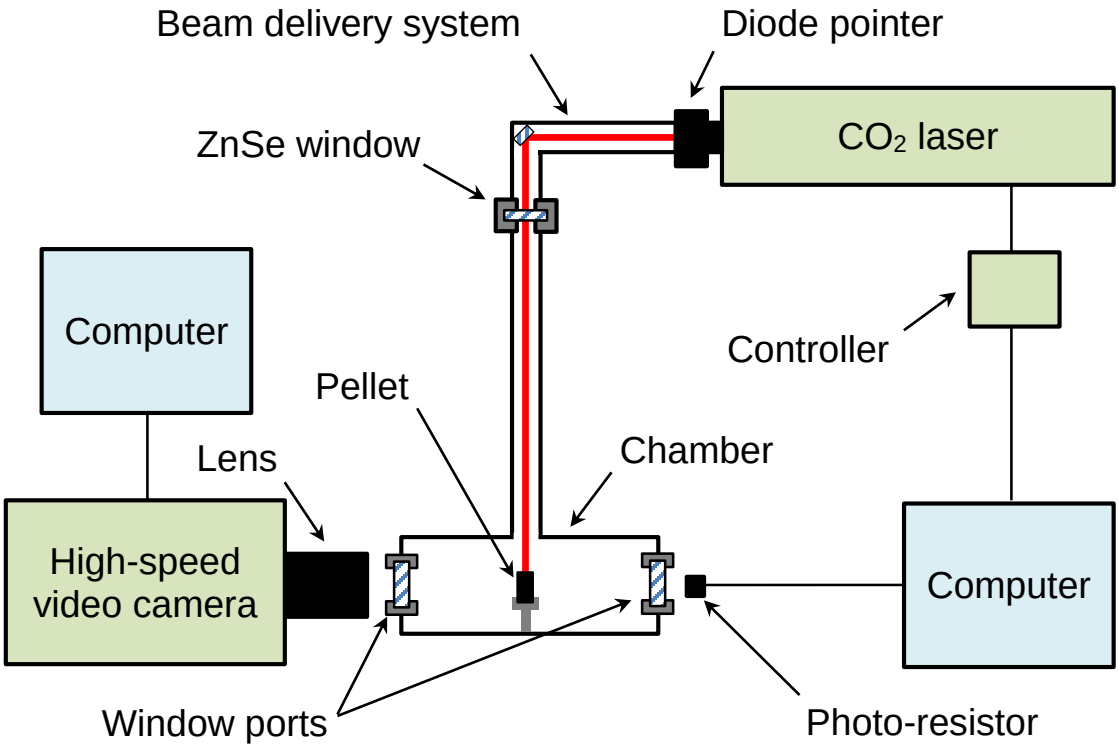

Figure 4.3: Schematic of new experimental combustion setup

The beam diameter at the top of the pellet is about 3 mm. Before every experiment the pellet is aligned with the infrared beam using a diode pointer (Synrad), which emits a visible red laser beam aligned with the CO_2 laser beam. The power of the CO_2 laser beam is controlled by a laser controller (Synrad UC-2000). In the reported experiments, the actual power of the beam after passing the beam delivery system and ZnSe window, measured with a power-meter (Synrad PW-250), was found to be 58−60 W. The duration of the laser pulse is set using a LabVIEW (National Instruments) software program that is in communication with the laser controller. A custom-made electronic arrangement based on a photo-resistor turns off the laser pulse upon the ignition of the sample. The ignition energy was calculated as the product of the beam power and the laser pulse duration. After ignition, the combustion front propagates downward

along the pellet. A high-speed video camera (Vision Research Phantom v1210), equipped with a lens for macro shooting (Nikon AF Micro NIKKOR 60mm f/2.8D), was used for observations of the combustion process and measurements of the front velocity. In the present research, the resolution was 1024x768 and the frame rate was varied from 1000 to 7000 fps.

4.4 Characterization of products

X-ray diffraction analysis were performed in order to examine and determine the composition of the combustion products of the iodine-containing thermite mixtures. Figure 4.4 shows the used instrument (Bruker D8 Discover XRD with Cu K-alpha radiation). The powdered combustion products were collected by scraping the walls of the combustion chamber and from within the sample holder, they were then analyzed at different 2θ values, ranging from 20° to 90°.

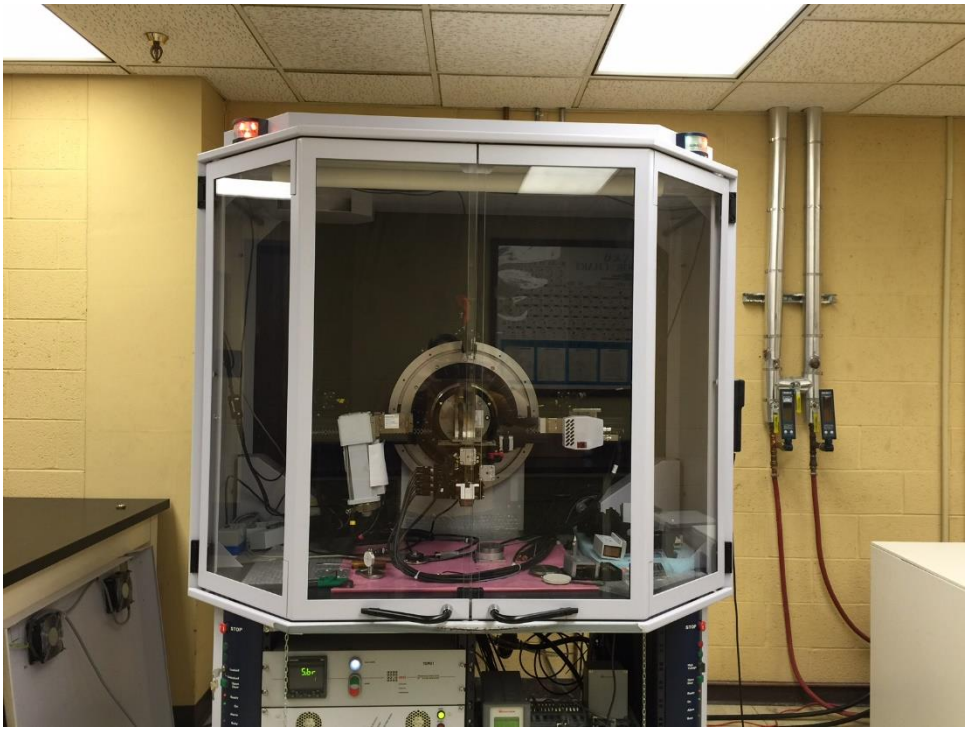

Figure 4.4: Bruker D8 Discover XRD

4.5 Chemical analysis

After every combustion experiment with iodine-containing pellets, the chamber is left to cool off for approximately 10 minutes. After this time, the chamber is taken from the setup and one lid is removed by unscrewing the four lid bolts, the brass sample holder is then removed and approximately 50 ml of toluene is poured into the chamber and the lid is placed back and secured with its bolts. In order to get as much product material for analysis, the chamber is shaken and agitated for about 3 minutes allowing the toluene to accumulate the products. One lid of the chamber is again removed and the toluene with the products is collected into a plastic container.

The collected solution of products contain various solid accumulations of material such as molten Al and Cu. Vacuum filtration is used to remove the undesired material. Figure 4.5.1 shows a schematic of the setup for this filtration process. The collected solution is poured gradually into the Buchner funnel through the filter paper to separate the solid materials. The obtained filtrated solution is then placed into an Erlenmeyer flask to be titrated.

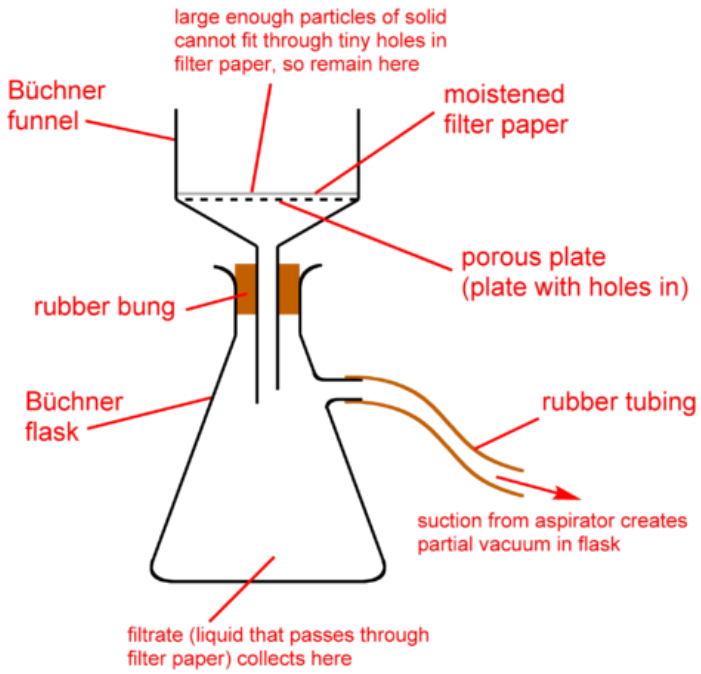

Figure 4.5.1: Schematic of vacuum filtration setup for combustion products solution

Sodium thiosulfate solution (0.05M) is used as the titrant for the chemical analysis of the filtrated combustion products. A burette is secured on a clamp and base, then it is properly rinsed three times and filled with the sodium thiosulfate solution until the measure on it its zero. The Erlenmeyer flask containing the products is then placed on the base below the burette and a piece of white paper is placed under the flask to help visualize the color change during the titration. Figure 4.5.2 shows this setup. The burette is then opened and the sodium thiosulfate is let into the Erlenmeyer flask slowly. As the sodium thiosulfate solution is poured, the flask is lightly stirred alloying for a better mixing of the products solution and the sodium thiosulfate; this is done until a clear end color is reached in the flask. When the clear end is reached, the volume on the burette is recorded. This process is performed 3 times for each mixture combustion products solution, therefore three final burette volumes are recorded and used to calculate the molarity of the products solution and consecutively the quantity of iodine in the solution.

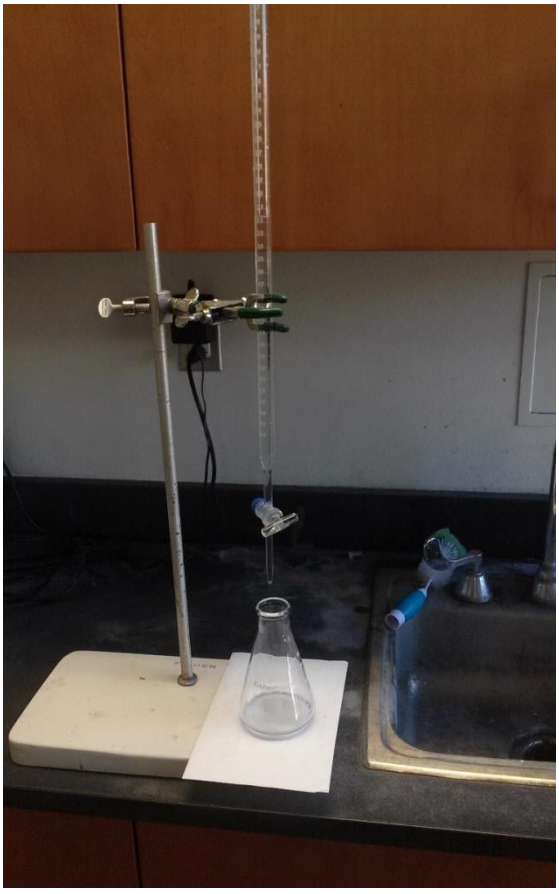

Figure 4.5.2: Titration setup for combustion products solution

4.6 Summary

Mechanically alloyed Al-I_2 powder was mixed with oxides Fe_2O_3, CuO, MoO_3, Bi_2O_3, and I_2O_5 to prepare thermite samples for combustion experiments. The same oxides were also mixed with conventional Al powder for a comparative study. Particle size distributions of all powders were determined using a multi-laser particle size analyzer. Al and Al-I_2 powders were mixed with the oxides according to the stoichiometries of Al-oxide reactions. For Al-I_2 based mixtures, iodine was considered to be an inert additive and the Al-I_2 mass required for stoichiometric mixture was determined knowing that Al is 80% of the Al-I_2 powder.

Samples were prepared by wet mixing in hexane and placed in an acoustic mixer at 40% intensity for approximately 2 minutes, the wet mixture was then put under vacuum to remove the hexane, leaving a dry powder mixture. The mixtures were then compressed into cylindrical pellets.

Pellets were ignited using a CO_2 laser. During the test, the laser beam directed to the top of the pellet heated the sample until ignition was achieved and then was turned off automatically. A high speed camera was used for video recording of the combustion process and subsequent determination of the front velocities.

X-ray diffraction analysis was used to characterize the combustion products. A wet chemical analysis was also performed, where titration was used to quantify the amount of iodine in the combustion products.

Chapter 5: Results and Discussion

5.1 Combustion behavior and characteristics

The combustion of iodine-generating thermite mixtures based on mechanically alloyed aluminum-iodine (Al-I_2) was studied. Based on stoichiometric ratios described in the previous chapter, the following reactive compositions were tested: Al-I_2/Fe_2O_3, Al-I_2/CuO, Al-I_2/Bi_2O_3, Al-I_2/MoO_3, and Al-I_2/I_2O_5. Along with these compositions, all metal oxides studied were also mixed with ordinary miron-sized aluminum for comparison. The mixtures were prepared using wet mixing in a vibration-acoustic mixer and compacted into cylindrical pellets. Ignition was performed inside an aluminum combustion chamber with the use of a CO_2 laser.

Several experiments were conducted with each of the thermite mixtures. High speed videos were obtained of the combustion of the mixtures and used for analysis. Figure 5.1 (see the next page) shows still images from some of the recorded videos.

The mixtures of Al-I_2 and Fe_2O_3 powders did not ignite. The laser hit the top of the pellet creating a luminous zone spot, but this one did not expand, i.e. the reaction did not propagate. The only observed effect of the laser heating was the ejection of fragments from the top of the pellet (see third image from row A in Figure 5.1), followed by fracturing and destruction of the pellet.

The mixtures of Al-I_2 with MoO_3, Bi_2O_3, and CuO powders easily ignited and burned in a self-sustained manner with average front velocities that varied in the range of 6 – 18 mm/s. The lowest velocity and unsteady phenomena propagation were observed during the combustions of Al-I_2/ MoO_3 mixtures pellets, Figure 5.1(E). On the other hand, mixtures with Bi_2O_3, and CuO exhibited a steady propagation front as seen in Figure 5.1(B and C).

The mixtures of Al-I_2 and I_2O_5 powders also burned in a steady manner with front velocities ranging from 13 to 16 mm/s. It was observed that the combustion area looked different when compared to the other thermite systems. Instead of a uniform luminous zone, the combustion front consists of numerous hot spots, separated from each other. Incandescent fragments were observed being ejected from the combustion area in the pellet, leading to the full dispersion of the material. This behavior can be observed in Figure 5.1(D).

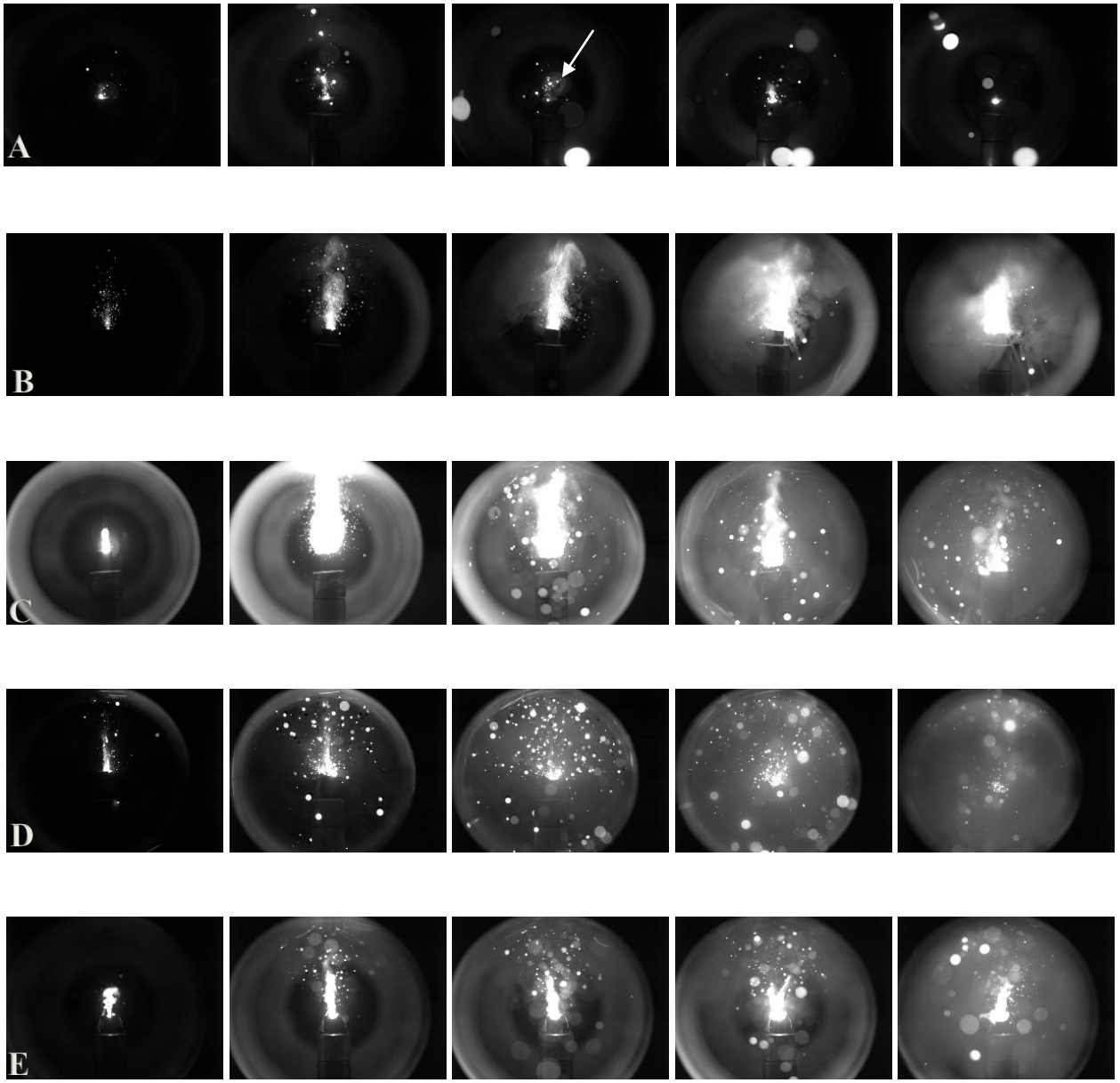

Figure 5.1: Progressive combustion still images of iodinated (Al-I_2) thermite samples. (A) Fe_2O_3, (B) Bi_2O_3, (C) CuO, (D) I_2O_5, (E) MoO_3

In the comparative experiments with mixtures based on commercial aluminum powder and the same metal oxides, MoO_3, Bi_2O_3, and CuO, a much faster combustion was observed, the front velocities on average exceeded 100 m/s. In contrast, it was found that the combustion of the mixture of Al and I_2O_5 powders was relatively slow and unsteady when compared to the mixture with Al-I_2, averaging a velocity of 5 mm/s.

Table 5.1 shows the relative densities for the studied mixtures and the measured velocities of combustion front propagation. The front propagation velocities were obtained by analyzing the movement of the propagating front from frame to frame and accounting for the recording speed, e.g., the number of frames per second. No reliable conclusions were made based on the ignition delays as they varied for the different mixtures in the range of 0.01 – 0.4 s; this was attributed to the variation of the mixture pellet absorptivity.

Table 5.1: Characteristics of studied thermite mixtures

Oxidizers	**Al-I_2**		**Al**	
	Relative density, %	Front velocity, mm/s	Relative density, %	Front velocity, mm/s
Fe_2O_3	59 – 83	No ignition	No test	No test
MoO_3	66 – 74	6	71 – 72	>100
Bi_2O_3	71 – 76	10	71 – 77	>100
CuO	66 – 85	13 – 18	72 – 74	>100
I_2O_5	84 – 86	13 – 16	73 – 90	~ 5

5.2 Products characterization

5.2.1 Materials particle size

A study of the particle size distribution was done for the materials used in the experiments, this was done to achieve a better understanding of the combustion results obtained. Figure 5.2.1 and Table 5.2 present data on the particle size distributions obtained for the used fuels and oxidizers. In the table, included are the mean volume diameter d_{mv}, the mean diameter d_{50}, and parameters d_{10} and d_{90}. It is seen that mechanically alloyed Al-I_2 powder is coarser than the commercial Al powder, which is characterized by a mean volume diameter of about 8 μm. The Al-I_2 powder and oxides of Cu and Mo had similar distributions, the mean volume diameters of these three powders were in the range from 20 to 30 μm.

Bismuth and iron oxides were finer with a 4 µm mean volume diameter for the former and 10 µm for the latter. Iodine pentoxide was the coarsest powder, with a mean volume diameter of about 70 µm.

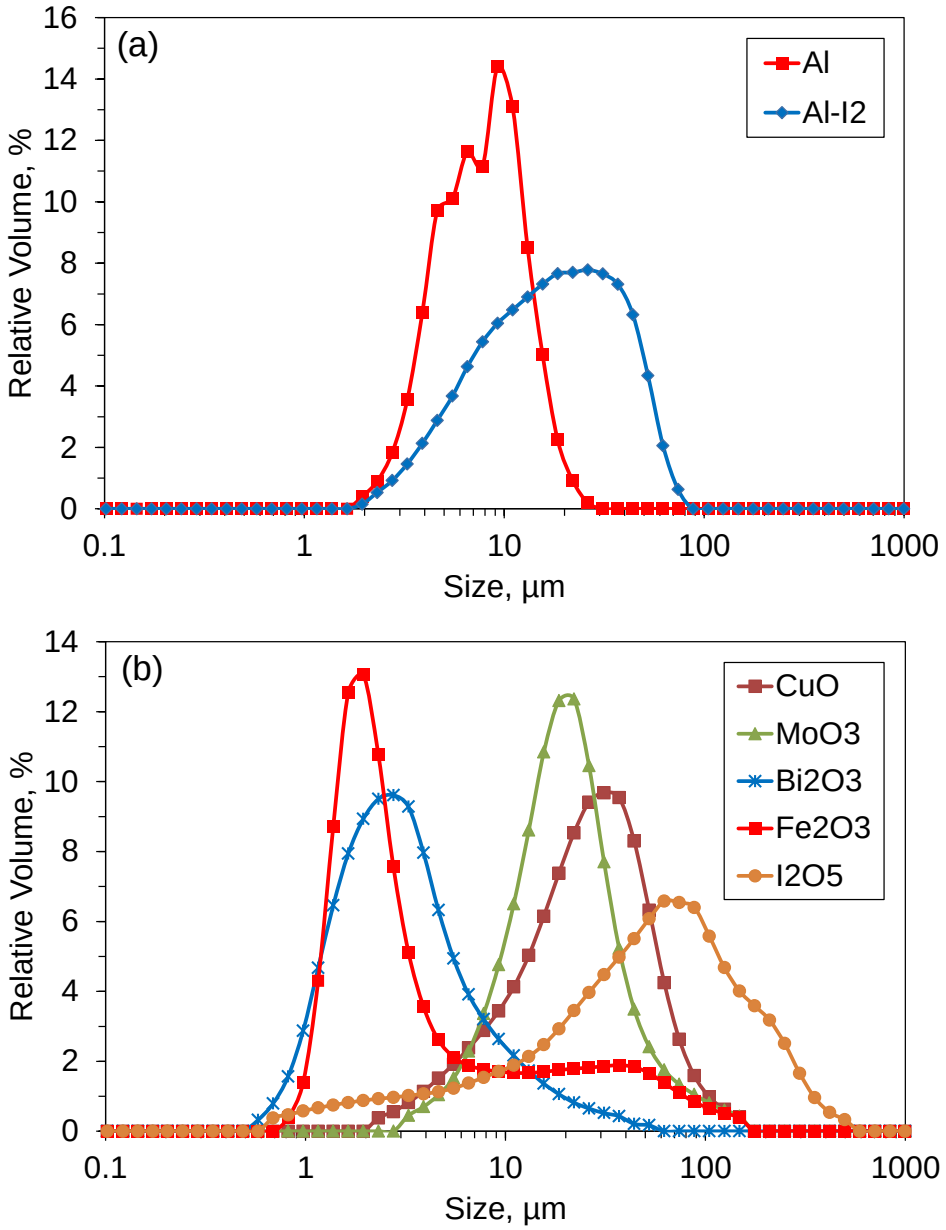

Figure 5.2.1: Particle size distributions of the used (a) fuels and (b) oxidizers.

Table 5.2: Particle size distribution of used fuels and oxidizers

Studied powders	d_{mv}, μm	d_{10}, μm	d_{50}, μm	d_{90}, μm
Al	7.70	3.62	7.15	12.57
Al-I_2	19.76	5.09	16.8	40.34
CuO	28.07	7.09	23.60	53.23
MoO_3	22.58	7.99	17.90	40.27
Bi_2O_3	4.24	1.148	2.621	8.69
Fe_2O_3	10.24	1.264	2.265	31.84
I_2O_5	69.90	4.85	47.53	168.9

5.2.2 X-ray diffraction

Condensed combustion products were collected from the combustion chamber and characterized using X-ray powder diffraction analysis. Since Al-I_2/Fe_2O_3 mixture did not ignite and Al/MoO_3 mixture was found to perform the worst among the others, it was decided to study only the XRD patterns for Al-I_2/CuO, Al-I_2/I_2O_5, and Al-I_2/Bi_2O_3 thermites products. These are presented in Figures 5.2.2 − 5.2.4.

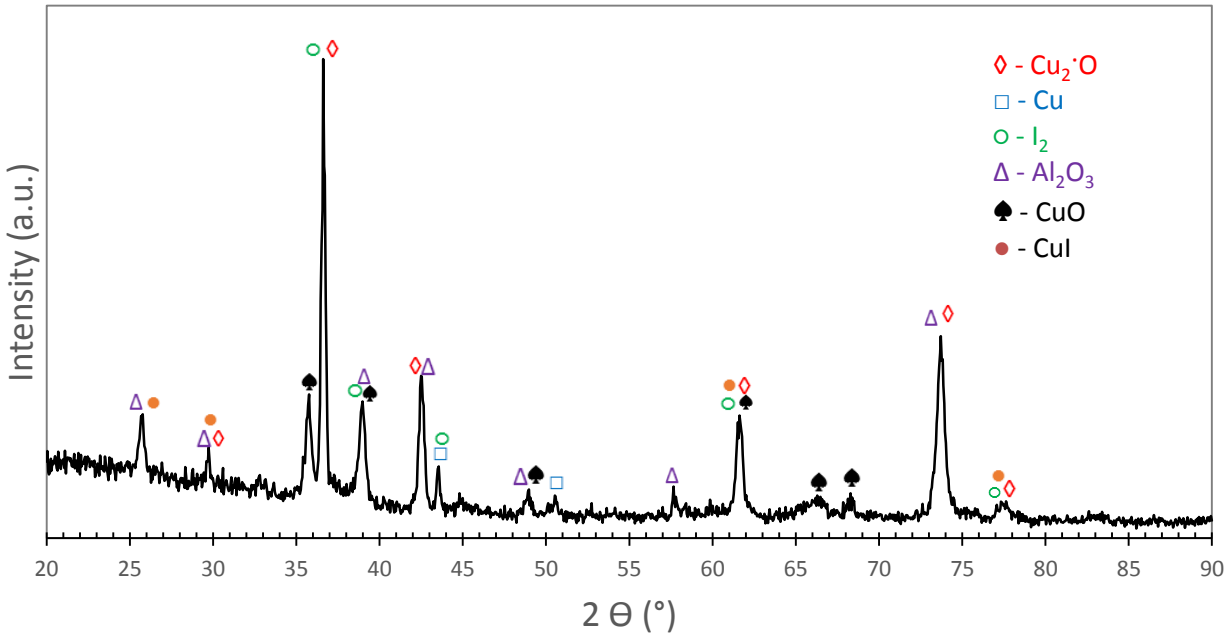

Figure 5.2.2: XRD pattern of combustion products for Al-I_2/CuO sample.

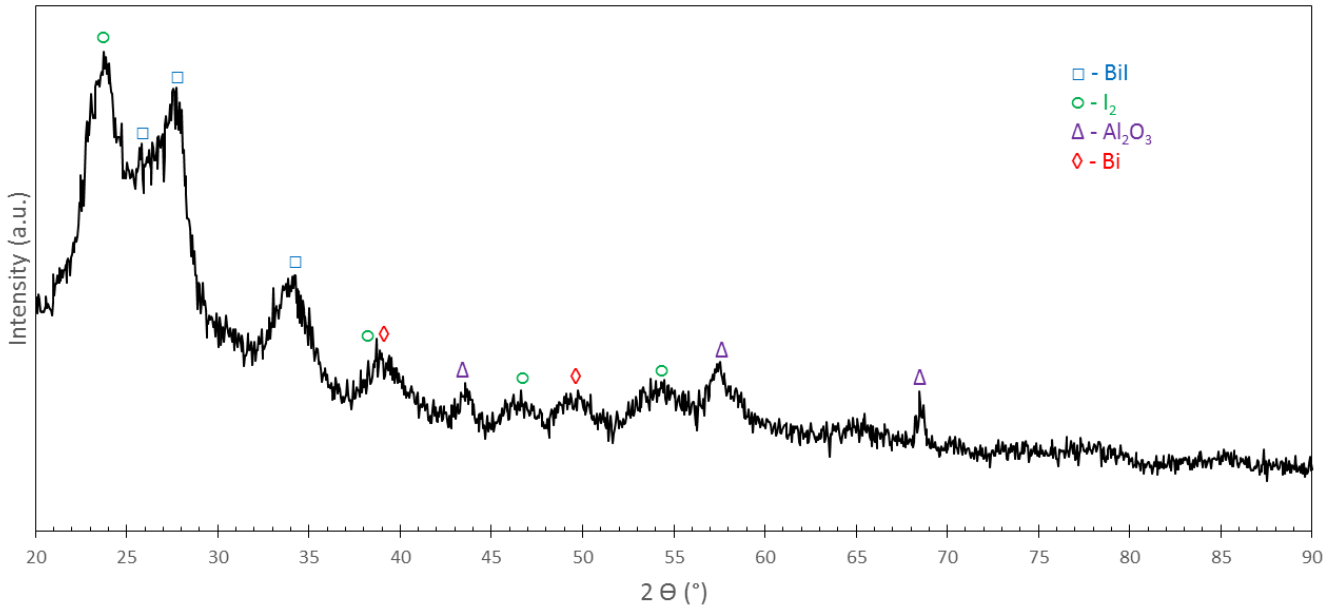

Figure 5.2.3: XRD pattern of combustion products for Al-I_2/ Bi_2O_3 sample.

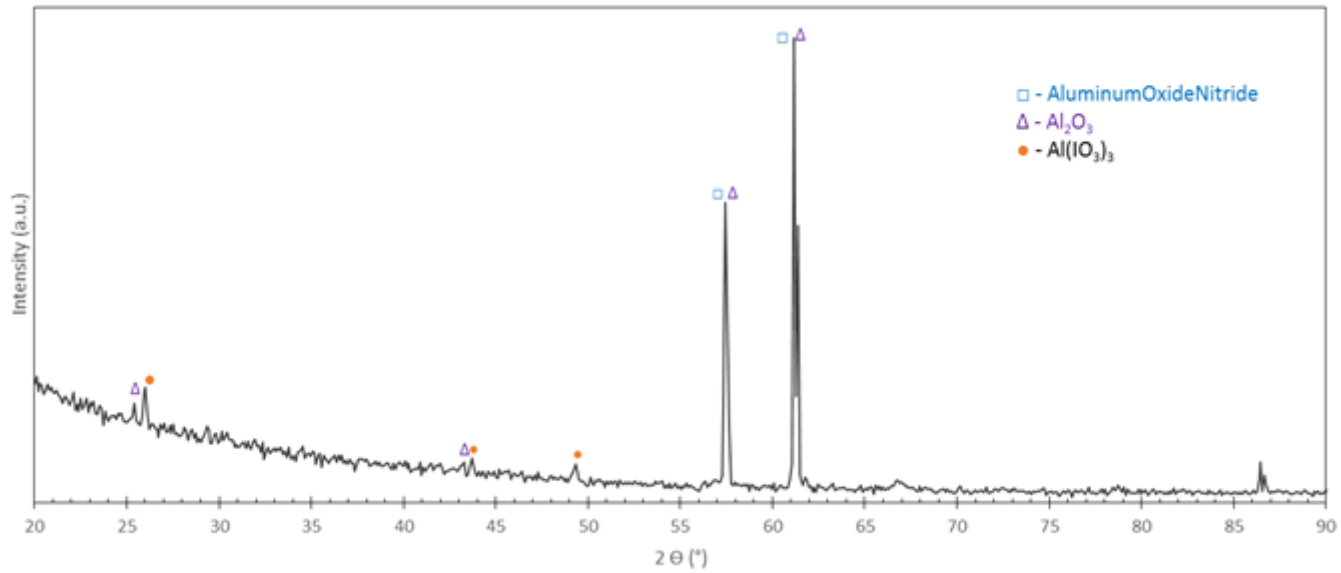

Figure 5.2.4: XRD pattern of combustion products for Al-I_2/I_2O_5 sample.

In all three XRD patterns, no Al peaks are seen, but there are peaks of Al_2O_3. This implies that Al was fully oxidized. The presence of Al_2O_3 also corroborates with results found on efforts where the

products of Al-based thermites with the same oxidizers were studied [17, 22]. The characterization of peaks in all three of the studies was complex as many of the peaks were conformed of various elements, e.g. peak at ~62° in Figure 5.2.1, and at ~39° in Figure 5.2.3. It is desired to find pure iodine elements in the combustion products as these contain the biocidal properties.

XRD patterns for the combustion products of CuO-based thermites (Fig. 5.2.2) show that I_2 may be present in three of the main peaks, but these peaks may also be caused by other phases (e.g., Cu_2O), which brings uncertainty to these results. Also, the presence of copper oxides implies that the combustion of the sample was not complete and that the full oxidation of Al may be caused by its reaction with atmospheric oxygen. Note, however, that some of the peaks (25°, 30°, and 62°) may indicate the presence of a copper-iodine compound (CuI) which also has biocidal properties.

For Bi_2O_3-based thermites (Fig. 5.2.3), iodine and BiI are present in the majority of the stronger peaks, The absence of bismuth oxide and the presence of Bi, Al_2O_3, BiI, and I_2 imply that the combustion was complete.

The XRD pattern for the combustion products of I_2O_5-based thermites (Fig. 5.2.4) shows a small number of peaks, which were identified as Al_2O_3, aluminum oxide-nitride, and $Al(IO_3)_3$. This indicates a high degree of conversion during combustion of this mixture. Nitride could form by the reaction of Al with atmospheric nitrogen though its presence cannot be reliably proven. In contrast with two other mixtures, no peaks that could indicate elemental iodine were found in the XRD patterns.

Interestingly, for all three thermite products characterized, no AlI_3 peaks were identified, while previous studies on the combustion of Al-I composites revealed presence of this phase in the combustion products [10-11].

5.2.3 Chemical analysis

After the combustion of iodine-containing thermite mixtures, the chamber was opened up and toluene was used to collect the combustion products. The collected solution was filtrated in order to remove solid products. Then a chemical titration was performed on the products solution employing sodium thiosulfate as the titrant, the results of the titration were used to find the amount of iodine release.

In order to prove the validity of this analysis, a titration was performed where a known quantity of iodine (0.15g) was dissolved into 50mL of toluene and the solution was titrated with sodium thiosulfate (0.05M). Three titrations were conducted and the titrant volumes used to reach a clear end were recorded. The average of these three volumes was calculated (12.36mL) and used to find the molarity and, in turn, the mass of iodine in the solution, as shown below in Equation 5.2.3.

$$0.01236L\left(\frac{.05\ mol}{1\ L}\right)\left(\frac{1\ mol\ I_2}{1\ mol\ Na_2S_2O_3}\right)\left(\frac{254\ g\ \ I_2}{1\ mol\ \ I_2}\right) = \ 0.157\ grams \tag{5.1}$$

The resultant mass for the titration is very close to the known iodine mass added to the toluene. The fact that it came out to be a slightly greater mass could be attributed to overshooting the volume of sodium thiosulfate during titrating because it is hard to precisely detect the point of reaching a clear end. Nevertheless, the titration seems to be an accurate method of quantifying the iodine found in the combustion products.

The expected amounts of iodine in the combustion products of thermites based on metal oxides are much less than for those of I_2O_5-based thermites. Since the samples in the present study were relatively small, a chemical titration analysis was performed on combustion products from the Al-I_2/I_2O_5 thermite. The average amount of iodine contained in one Al-I_2/I_2O_5 sample was approximately 0.86g. The average titrant volume used to reach a clear end was 11.7mL. The mass of iodine in the products solution was then calculated using the same process as in Equation 5.2.3. This mass was found to be equal to 0.8g, which is close to the known mass, 0.86g. This demonstrates the effectiveness of using titration analysis for the quantification of iodine in the combustion products of thermites.

5.3 Discussion

The experiments have shown that the front velocities in all mixtures with Al-I_2 powder are similar to one another, despite different chemical compositions and particle sizes of the oxidizers tested. This indicates that the reaction might be controlled by the processes related to the metal particles. Prior studies [27] have shown that low temperature oxidation of Al particles is controlled by outward diffusion of Al ions to the exterior of the oxide shell covering the metal. It is possible that this process also controls the

reaction between Al-I_2 and metal oxide particles during propagation of the combustion wave over the mixture.

Further, the experiments have shown that the front velocities in the mixtures with Al-I_2 powder and metal oxides are much lower than those for the mixtures of the same oxides with a commercial, micron-sized Al powder. To verify that this effect is not caused by the decrease in the combustion temperature due to the addition of iodine, the adiabatic flame temperatures of all studied mixtures were calculated for 1 atm pressure using THERMO software [28]. The formation enthalpy of I_2O_5, -157.92 kJ/mol [29], was added to the database. It was assumed in the calculations that Al-I_2 material was just a mixture of Al and I_2. The results have shown that the replacement of Al with Al-I_2 decreases the adiabatic flame temperature of all mixtures by 11 – 80 K. Such a small reduction in the temperature cannot justify the significant decreases in the velocity of front propagation observed for the thermites based on metal oxides.

Table 5.3. Adiabatic flame temperatures of the tested mixtures.

Oxidizer	**Adiabatic Flame Temperature, K**	
	Al	**Al·I_2**
Fe_2O_3	3131	3051
MoO_3	3808	3738
Bi_2O_3	3284	3234
CuO	2838	2823
I_2O_5	3827	3816

The decrease in the front velocity may be associated with a larger size of mechanically alloyed Al-I_2 powder as seen in Table 5.2. In a recent study on the ignition mechanisms of thermites [30], the investigated mixtures included nano-scale Al and different metal oxides including four of the metal oxides studied in the present work. It was shown that at least for the thermites based on MoO_3, Bi_2O_3, SnO_2, Sb_2O_3, and WO_3, the ignition is likely a result of direct interfacial contact between fuel and oxidizer,

leading to condensed state mobility of reactive species, rather than a result of reaction with gaseous oxygen released form the meatal oxides. Apparently the same mechanism takes place during ignition of all thermites studied in the present work, except for I_2O_5-based mixtures. Since Al-I_2 powder is coarser than the tested Al powder, it has a lower area of contact with the oxide, which decelerates the reaction between the metal and the oxide particles.

The non-ignition of Al-I_2/Fe_2O_3 mixtures correlates with the high ignition temperature of Al/ Fe_2O_3 thermite as compared with those of other aluminum metal oxide thermites [30]. This results corroborate the findings by Sullivan et al. [17] where they characterized Fe_2O_3 as a relatively poor oxidizer. The behavior observed has also been reported in other papers, Johnson et al. [31] found that the combustion of micron-sized Al/ Fe_2O_3 produced a dispersion of particles upon ignition, this problem was addressed by adding excess metal ingredient (Fe) up to 40% of the mixture which reduced the reaction temperature of the system.

The mechanism of oxygen transport to metal particles during combustion of I_2O_5-based thermites is probably different. It is known that iodine pentoxide decomposes to O_2 and I_2 at a relatively low temperature of about 400°C [32]. Thus, it is likely that the reaction does not happen at the particle-particle interface, but rather in the gas phase. It has been observed earlier that at such temperatures, mechanically alloyed Al-I_2 powder rapidly reacts with gaseous oxygen [11, 12]. Combustion of the Al-I_2/ I_2O_5 mixtures may still depend on the outward diffusion of Al through the particle oxide shells, but the observed different structure of the combustion front (hot spots rather than a uniform luminous zone) supports the hypothesis of a different combustion mechanism.

These considerations also explain the observed slow and unsteady combustion of Al/ I_2O_5 thermite. Oxidation of conventional micron-sized Al powder begins at a higher temperature than for the mechanically alloyed Al-I_2 powder. The temperature at which significant oxidation of Al begins, I_2O_5 is already expected to have decomposed. Therefore, in the prepared powder mixtures, the zones of I_2O_5 decomposition and Al oxidation in the combustion wave may be spatially separated, causing a decrease in the front velocity.

5.4 Summary

The mixtures of Al-I_2 and Fe_2O_3 powders did not ignite. The mixtures of Al-I_2 with I_2O_5, Bi_2O_3, and CuO exhibited similar front propagation velocities, in the range of 10 mm/s to 18 mm/s, while MoO_3–based mixtures had the slowest front velocity at ~6 mm/s along with an unsteady front propagation. It was also observed that the combustion front velocities for conventional Al-based mixtures were much faster (>100 mm/s) than for Al-I_2 mixtures; this was observed with mixtures composed of metal oxides (i.e. MoO_3, Bi_2O_3, and CuO). On the contrary, for mixtures containing I_2O_5, the combustion front velocity was faster for Al-I_2 mixtures than for conventional Al ones. Also for Al-I_2/I_2O_5 mixtures, the combustion behavior was seen to be different from that for Al-I_2 mixtures with metal oxides. These observations lead to the assumption that two different combustion mechanisms were taking place for Al-I_2 mixtures, one for metal-oxide based mixtures and the other one for I_2O_5 mixtures.

It has been demonstrated in previous studies that for metal oxide based thermites, the ignition is a result of direct interfacial contact between the metal fuel and the oxidizer. Since Al-I_2 was found to be coarser than the conventional Al used for the comparative studies, the smaller size of Al creates a more homogeneous mixture with more contact points between the fuel and the oxidizer than inj the case of Al-I_2 mixtures. A slower reaction and combustion propagation is to be expected for Al-I_2 based mixtures.

The reaction between Al-I_2 and I_2O_5 seems to occur in a gas phase instead of the condensed particle-to-particle behavior observed for the other oxidizers. It is know that I_2O_5 decomposes to O_2 and I_2 at relatively low temperatures (390°C). A recent study showed that Al-I_2 ignites in O_2 gas environment at approximately the same temperature range in which I_2O_5 decomposes, while micron-sized Al ignites at a much higher temperature. This may explain why Al-I_2/ I_2O_5 mixtures burn more rapidly than Al/I_2O_5 mixtures.

X-ray diffraction analysis was performed on the products of the Al-I_2/Bi_2O_3, Al-I_2/CuO, and Al-I_2/I_2O_5 mixtures as these showed the most promising combustion characteristics. The products for Bi_2O_3 based mixtures showed the absence of Bi_2O_3 and the presence of Al and Bi, implying that the combustion was complete. Pure I_2 and BiI were also found in the products. For Al-I_2/CuO mixtures various copper oxides were encountered in the combustion products indicating that the combustion was not fully completed. I_2 and

CuI might be present in the products as well. Note that CuI has been shown to also possess biocidal properties. Surprisingly, elemental iodine was not found in the combustion products of the Al-I_2/I_2O_5 mixtures; $Al(IO_3)_3$ was the only iodine-containing product.

A validation study was performed for the chemical analysis used for the quantification of iodine released. The titration method with sodium thiosulfate was shown to be an accurate process for quantification of iodine contained in the solution of toluene and combustion products. Titration analysis of solutions containing the combustion products of Al-I_2/I_2O_5 mixtures revealed that the amount of iodine in the products is 0.84 g, while the calculated amount of iodine contained in an Al-I_2/I_2O_5 sample was 0.86 g. Since these values are close to each other, it is suggested that the release of iodine during combustion is effective.

Chapter 6: Conclusion

The design and construction of a new chamber has enabled efficient combustion experiments with iodine-generating thermites. The accessibility of the chamber allowed for faster and easier sample introduction and products collection. In particular, the chamber's relatively small volume facilitated the collection of products in toluene for subsequent analysis. The chamber was also successful at containing combustion gases from exiting to the surroundings.

Modifications on the laser ignition setup such as the physical kill-switch and alerting revolving light improved the safety. The addition of the photo-resistor created a more effective laser ignition system in which the laser would be prevented from assisting the combustion once ignition was reached.

A setup addition which would improve the experimental capabilities would be a system for measuring the ignition delay time of the sample, i.e. the time it takes for the sample to ignite from the moment the laser hits the top of the pellet. This knowledge would allow for the calculation of energy required to ignite a sample. Also, it would be beneficial to modify the setup in order to have temperature readings along the sample. An approach to these would be the modification of the chamber that allows the introduction of thermocouples without compromising the capability of the chamber to contain combustion gases.

The experiments have been conducted with mixtures of mechanically alloyed Al-I_2 powder with Fe_2O_3, CuO, MoO_3, Bi_2O_3, and I_2O_5. Mixtures based on Fe_2O_3 do not ignite, while mixtures based on the other oxides exhibit a self-sustained propagation of the combustion front with similar burn rates. Comparison experiments with a finer, micron-sized Al powder have shown a more rapid combustion for mixtures based on metal oxides. In contrast, a slower and unsteady combustion was observed for Al-I_2/ I_2O_5 thermite.

Similar burn rates for thermites with Al-I_2 mixed with different oxides indicate that the reaction is controlled by outward Al diffusion through the oxide shells of the metal particles. In mixtures with metal oxides, the reaction requires interfacial contact between the fuel and oxidizer, so that replacing Al-I_2 with a finer Al powder increases the reaction rate. In contrast, in mixtures with iodine pentoxide, aluminum reacts with gaseous oxygen released by the oxide decomposing at a lower temperature. Since oxidation of

Al-I_2 and decomposition of I_2O_5 occur in the same temperature range, Al-I_2/ I_2O_5 mixtures burn rapidly. In contrast, Al/ I_2O_5 mixtures exhibit a slow and unsteady combustion because the oxidation temperatures of the micron-sized Al powder are higher than the decomposition temperature of I_2O_5.

Solid combustion products for mixtures of the mechanically alloyed Al-I_2 powder with CuO, Bi_2O_3, and I_2O_5 were characterized by XRD diffraction analysis. The XRD results revealed full oxidation of Al for all three mixtures, which, however, may also be related to its oxidation by atmospheric oxygen. The XRD pattern of the product for CuO-based mixture contained peaks of copper oxides, which indicates incomplete conversion.

The combustion products for Al-I_2/I_2O_5 were analyzed with the chemical titration analysis and a very close value to the expected amount of iodine was found in the products solutions. Thus, it was shown that the titration analysis is an accurate iodine quantification method for the combustion products of iodine-containing mixtures.

References

[1] "USA Department of Homeland Security", 2004. [Online]. Available: https://www.dhs.gov/xlibrary/assets/prep_chemical_fact_sheet.pdf

[2] "International Committee of the Red Cross", [Online]. Available: https://www.icrc.org/ihl/INTRO /195

[3] "BBC UK News", [Online]. Available: http://news.bbc.co.uk/onthisday/hi/dates/stories/march/16/newsid_4304000/4304853.stm

[4] J. W. Jones; Lockheed Martin Corporation, "Agent Defeat Warhead Device". United States patent US 6,382,105 B1. 2002 May 7.

[5] B.R. Clark, and M.L. Pantoya, "The aluminium and iodine pentoxide reaction for the destruction of spore forming bacteria", *Physical Chemistry Chemical Physics,* vol. 12, pp. 12653–12657, 2010.

[6] S.A. Grinshpun, A. Adhikari, M. Yermakov, T. Reponen, E.L. Dreizin, M. Schoenitz, V. Hoffmann, and S. Zhang, Environ. Sci. Technol. 46, pp. 7334–7341, 2012.

[7] S.A. Grinshpun, C. Li, A. Adhikari, M. Yermakov, T. Reponen, M. Schoenitz, E. Dreizin, V. Hoffman, and, M. Trunov, "Method for studying survival of airborne viable microorganisms in combustion environments: development and evaluation", *Aerosol and Air Quality Research,* vol. 10, pp. 414–424, 2010.

[8] Y. Aly, S. Zhang, M. Schoenitz, V.K. Hoffmann, E.L. Dreizin, M. Yermakov, R. Indugula, and S.A. Grinshpun, "Iodine-containing aluminum-based fuels for inactivation of bioaerosols", *Combustion and Flame,* vol. 161, pp. 303–310, 2014.

[9] C.E. Johnson, and K.T. Higa, "Iodine-rich biocidal reactive materials", MRS Online Proc. Libr. 1521, (2013), doi:10.1557/opl.2013.46.

[10] S. Zhang, M. Schoenitz, and E.L. Dreizin, "Mechanically alloyed Al–I composite materials", Journal of *Physics and Chemistry of Solids*, vol. 71, pp. 1213–1220, 2010.

[11] S. Zhang, M. Schoenitz, and E.L. Dreizin, "Iodine release, oxidation, and ignition of mechanically alloyed Al-I composites, *Journal of Physics and Chemistry of Solids,* C114, pp. 19653–19659, 2010.

[12] S. Zhang, C. Badiola, M. Schoenitz, and E.L. Dreizin, "Oxidation, ignition, and combustion of Al-I_2 composite powders", *Combustion and Flame*, vol. 159, pp. 1980–1986, 2012.

[13] R.A. Yetter, G. A. Risha, S. F. Son, *Proceedings of the Combustion Institute,* vol. 32, pp. 1819-1838, 2009.

[14] D.S. Wen, *Energy Environmental Science,* vol. 3, pp. 591-600, 2010.

[15] S. Bless, R.Russell, and M.Pantoya, "Impact-driven reactions in biocidal reactive materials for weapons of mass destruction (WMD) applications", Annual Progress Report to the Defense Threat Reduction Agency, Austin, 2011.

[16] "World Public Libray", 2002. [Online]. Available: http://www.worldlibrary.org/article/ whebn0000439879/1893%20in%20science#cite_note-0

[17] K.T. Sullivan, N.W. Piekiel, S. Chowdhury, C. Wu, M.R. Zachariah, and C.E. Johnson, "Ignition and combustion characteristics of nano scale Al/AgIO3: a potential energetic biocidal system", *Combustion Science Technology*, vol. 183, pp. 285–302, 2011.

[18] J.J. Granier, K.B. Plantier, M. Pantoya, "The role of the Al2O3 passivation shell surrounding nano-Al particles in the combustion synthesis of NiAl", *Journal of Materials Science,* vol. 39, pp. 6421-6431, 2004.

[19] M.R. Weismiller, J.Y. Malchi, J.G. Lee, R.A. Yetter, T.J. Foley, *Proceedings of the combustion institute,* vol. 33, pp. 1989-1996, 2011.

[20] L. Glavier, G. Taton, J.M. Ducere, and V. Baijot, "Nanoenergetics as pressure generator for nontoxic impact primers: Comparison of Al/Bi_2O_3, Al/CuO, Al/MoO_3 nanothermites and Al/PTFE", *Combustion and Flame*, vol. 162, pp. 1813-1820.

[21] R. Russell, S. Bless, and M. Pantoya, "Impact-driven thermite reactions with iodine pentoxide and silver oxide", *Journal of Energetic Materials*, vol. 29, pp. 175–192, 2011.

[22] G. Jian, S. Chowdhury, J. Feng, and M. Zachariah, "The ignition and combustion study of Nano-Al and iodine pentoxide thermite", *Combustion Institute,* vol 2, 1287-1299, 2013.

[23] S.H.Fischer, M.C.Grubelich, *the 24th International Pyrotechnics Seminar*, Monterey, CA, July 1998.

[24] A. C. Larson, and R. B. Von Dreele, *Los Alamos National Lab.* Rept. LAUR 86-748, Los Alamos, NM, 2004.

[25] M. Machado, D. Rodriguez, Y. Aly, M. Schoenitz, E. Dreizin, and E. Shafirovich, "Nanocomposite and mechanically alloyed reactive materials as energetic additives in chemical oxygen generators", *Combustion and Flame*, vol. 161, pp. 2708-2716, 2014.

[26] D. Rodriguez, E. Dreizin, and E. Shafirovich, "Hydrogen generation from ammonia borane and water through combustion reactions with mechanically alloyed Al·Mg powder", *Combustion and Flame,* vol. 162, pp. 1498-1506, 2015.

[27] S. Zhang, and E.L. Dreizin, "Reaction interface for heterogeneous oxidation of aluminum powders", *Journal of Physics and Chemistry*, C117, pp. 14025–14031, 2013.

[28] A.A. Shiryaev, "Thermodynamics of SHS processes: An advanced approach", *International Journal of Self-propagating High-temperature Synthesis*, vol. 4, pp. 351–362, 1995.

[29] M.W. Chase, NIST−JANAF thermochemical tables for the iodine oxides, *Journal of Physics and Chemistry,* Reference Data 25, pp. 1297–1340, 1996.

[30] G. Jian, S. Chowdhury, K. Sullivan, and M.R. Zachariah, "Nanothermite reactions: Is gas phase oxygen generation from the oxygen carrier an essential prerequisite to ignition?" *Combustion and Flame*, vol. 160, pp. 432–437, 2013.

[31] C.E. Johnson, K.T. Higa, T. Tran, and W. R. Albro, "Thermite initiation processes and thresholds", *Materials Research Society,* vol. 1405, 2012.

[32] C. Farley, and M. Pantoya, "Reaction kinetics of nanometric aluminum and iodine pentoxide", *Journal of Thermal Analysis and Calorim*etry, vol. 102, pp. 609–613, 2010.

Vita

Sergio Emanuel Guerrero was born in El Paso, Texas, United States on September 5th, 1990. Mr. Guerrero attended Austin High School in El Paso. He enrolled at the University of Texas at El Paso in 2009, where he completed a Bachelor's of Science in Mechanical Engineering in 2013. During the Summer of 2013, Mr. Guerrero was an intern at NASA Goddard Space Flight Center working with two-phase heat transfer loop heat pipes for spacecraft applications under the supervision of Dr. Yentung Ku. Mr. Guerrero started his graduate studies at the University of Texas at El Paso pursuing a Master's Degree in Mechanical Engineering. He immediately began to work as a research assistant in the Center for Space Exploration Technology Research under the supervision of Dr. Evgeny Shafirovich. There, he worked for the DOD-sponsored project on the generation of biocidal gases from energetic mixtures. Based on Mr. Guerrero's results, an article titled "Combustion of thermite mixtures based on mechanically alloyed aluminum–iodine material" was published in the peer-reviewed journal *Combustion and Flame*. Mr. Guerrero presented his work at the 5th Southwest Energy Science and Engineering Symposium. His work was also presented at the 9th U.S. National Combustion Meeting. During his time as graduate student Mr. Guerrero also worked as a co-op at NASA Goddard Space Flight Center under the thermal engineering branch. There, he worked on the Wide Field Infra-Red Survey Telescope (WFIRST) performing thermal simulation analysis and on the 6U cube-sat Dellingr performing heat conduction and thermal mass studies.

Permanent address: 3420 Dundee St.
El Paso, Texas, 79925

This thesis was typed by Sergio Emanuel Guerrero.